THE ASTROPHYSICAL JOURNAL, 389:39–62, 1992 April 10

A SPECTROSCOPIC STUDY OF UM 673 A AND B: ON THE SIZE OF LYMAN-ALPHA CLOUDS[1]

A. SMETTE,[2,3,4] J. SURDEJ,[3,5] P. A. SHAVER,[2] C. B. FOLTZ,[6] F. H. CHAFFEE,[6,7] R. J. WEYMANN,[8]
R. E. WILLIAMS,[9] AND P. MAGAIN[3,5]

Received 1991 February 27; accepted 1991 September 10

ABSTRACT

We present a study of the Lyα forest spectra (2 Å resolution) obtained for the A and B images of the gravitationally lensed high-redshift quasar UM 673. We also present higher resolution data of the brightest (A) image. In the 2 Å resolution spectra, all the absorption lines detected at 5 σ in the spectrum of the fainter B image are present in the A image; however, we find two anticoincidences, i.e., two lines in A which do not have a counterpart in B at more than a 3 σ confidence level. Given the fact that corresponding Lyα lines in the spectra of A and B have their equivalent widths well correlated, this proves that both light beams actually cross the same clouds. Most of the velocity differences between corresponding lines are compatible with 0 km s^{-1} within the error bars, with a standard deviation of 17 km s^{-1}.

As the comoving linear separation increases from virtually $0h_{50}^{-1}$ kpc ($H_0 = 50h_{50}$ km s^{-1} Mpc^{-1}, $q_0 = 0$) at the redshift of the QSO to $2h_{50}^{-1}$ kpc, we derive a best value of $12h_{50}^{-1}$ kpc for the 2 σ lower limit and of $160h_{50}^{-1}$ kpc for the 2 σ upper limit of the diameter of spherical Lyα clouds in the redshift range 2.1–2.7, by means of Monte Carlo simulations. However, if we interpret the two anticoincidences as due to a Mg II doublet at $z = 0.4261$, we find in this case a best value of $23h_{50}^{-1}$ kpc to the 2 σ lower limit of the Lyα cloud diameter, but we cannot derive any upper limit.

For the two major heavy-element systems detected in the spectrum of UM 673, we do not find any significant difference between the corresponding lines in the two spectra, indicating that these systems do not show dramatic variations over scales of $0.8h_{50}^{-1}$ and $2.1h_{50}^{-1}$ kpc, respectively.

Subject headings: gravitational lensing — quasars: absorption lines — quasars: individual (UM 673)

1. INTRODUCTION

The study of gravitational lens systems not only provides us with a unique tool to derive an independent estimate of the Hubble parameter H_0 or the mass of the lensing galaxy and its associated cluster (Refsdal 1964) but also allows us to understand better the variations of the galactic or intergalactic medium over scales of the order of virtually zero to several kiloparsecs.

The most striking feature that appears in the blue wing of the Lyα emission line in the spectra of distant quasars is a forest of narrow absorption lines due to hydrogen clouds located along our line of sight (Sargent et al. 1980, hereafter SYBT). Various models have been invoked to describe their physical state: pressure-confined clouds in an expanding intergalactic medium (SYBT; Ikeuchi & Ostriker 1986), relics of primordial density fluctuations in the cold dark matter scenario for the biased formation of galaxies (Bond, Szalay, & Silk 1988), gravitationally confined clouds in cold dark matter minihalos (Rees 1986), or thermally unstable shocks associated with the formation of protogalaxies (Lake 1988; Hogan 1987). Despite these various possible scenarios for the origin of the Lyα clouds, there is still no general agreement on values of basic physical parameters such as their typical size.

SYBT observed that the Lyα absorption lines reach zero intensity even on the Lyα emission-line wings, in 0.8 Å resolution spectra. Following the argument given by Rees (1970), they concluded that the clouds cover the emission-line region of the QSO and set a *lower* limit of the order of 10 pc for their characteristic size.

In a spectral range of 900 Å between 3450 and 4350 Å, covering 400 Å of the Lyα forest, Foltz et al. (1984) found two or three Lyα lines which are not common or are of substantially different strengths in comparing 1 Å resolution spectra for the two images of Q2345+007 (separation 7.″3). Identifying the radius of a cloud with the separation between the light beams at the redshift ($z_a = 1.951$) of the shortest wavelength common line, they determine a lower limit of roughly $5h_{50}^{-1}$ kpc to $25h_{50}^{-1}$ kpc for the radius of the Lyα clouds.

However, noticing that the column density distribution functions for Lyα clouds and heavy-element systems could be fitted by the same power law, Tytler (1987) proposed that they form a single population. The fact that no metal lines are found in the Lyα systems requires that they have total column densities of 10^{17} cm^{-2} or less, or, for those with N(H I) $\sim 10^{17}$ cm^{-2}, that they be nearly neutral. In such a picture the Lyα clouds are small ($\leq 10^{18}$ cm) in general, with a wide variety of ionizations (and metal abundances up to 0.1 solar), while a few could be larger ($\sim 10^{21}$ cm) and of high ionization. To explain

1 Based on observations made at the MMTO, at ESO, and at the CTIO.

2 European Southern Observatory, Karl-Schwarzschild-Strasse, 2, D-8046 Garching bei München, Germany.

3 Institut d'Astrophysique, Université de Liège, Avenue de Cointe, 5, B-4000 Cointe, Belgium.

4 Now at European Southern Observatory, Casilla 19001, Santiago 19, Chile.

5 Also Chercheur Qualifié au Fonds National de la Recherche Scientifique (Belgium).

6 Multiple Mirror Telescope Observatory, Smithsonian Institution and the University of Arizona, Tucson, AZ 85721.

7 At Institute of Astronomy, Cambridge, England, from 1990 July to 1991 July.

8 Observatories of the Carnegie Institution of Washington, 813 Santa Barbara Street, Pasadena, CA 91101.

9 Cerro Tololo Inter-American Observatories, Casilla 603, La Serena, Chile.

the results of Foltz et al. (1984) most of the clouds should have high aspect ratios, of the order of 10^5 at least.

Recently, Pettini et al. (1990) obtained qualitatively the same conclusion about the size of the Lyα clouds: using a 6 km s^{-1} resolution spectrum of Q2206−199N and limiting themselves to low H I column density, they found that (1) most of the lines have a b parameter less than 22 km s^{-1}, (2) this b parameter is correlated with the cloud column density $N_{\rm H\,I}$ for log N(H I) $\simeq$ 12.7–14.0.

From the low observed values of b, they concluded that Lyα clouds must be cold, hence neutral and small (10^{-5} pc) or sheetlike objects. They interpreted the observed correlation by attributing the line broadening more to large scale rather than to thermal motion, implying that *all* Lyα clouds are cooler than previously thought. From this point of view, Pettini et al. (1990) consider the result of Foltz et al. (1984) as a typical clustering length instead of an estimation of the cloud size; they invoke a possible second population of Lyα clouds, characterized by a higher H I column density than the ones they selected, in order to explain that some lines reach zero intensity in the wings of the Lyα emission line.

It should be pointed out that, if spherical, isolated Lyα clouds actually had the size quoted by Pettini et al. (1990), the Lyα forest of a single quasar would look completely different from one year to the other simply because of the relative motion of Earth, as already argued by Rees (1970).

On the other hand, a similar work conducted by Carswell et al. (1991) on the quasar Q1100−264 leads to different results, i.e., (1) the b parameter ranges from 12 to 80 km s^{-1} (with a different line selection), but few lines have low Doppler parameters; (2) the correlation reported between the Doppler parameter and the H I column density is contested.

Here we present results of the analysis of spectra obtained for the UM 673 A and B images (cf. Surdej et al. 1987, hereafter Paper I; Surdej et al. 1988, hereafter Paper II). In comparison with the data of Foltz et al. (1984), our data are characterized by a better signal-to-noise ratio, and they cover a much larger spectral range (1700 Å), with 1400 Å in the Lyα forest, but at 2 Å resolution. An advantage of using the images of UM 673 as probes of the intergalactic medium is that the lens has been identified ($z_d = 0.493$), but on the other hand, the separation between the A and B images is more than 3 times smaller (2".22) than for Q2345+007. In the remainder we shall use the value of 2.727 for the redshift of UM 673 (cf. Sargent, Boksenberg, & Steidel 1988, hereafter SBS). Preliminary results of this study have been reported by Smette et al. (1990).

2. SPECTROSCOPIC OBSERVATIONS

2.1. *The* 1 *and* 2 Å *Resolution Spectra*

Observations of the UM 673 A and B images were obtained (by C. F. and F. C.) using the Blue Channel of the MMT Spectrograph equipped with an intensified photon-counting Reticon detector. Details of the dates of observations, exposure times, spectral coverage, and resolutions are given in Table 1. All observations were taken through a pair of 1" × 3" slits, with the long axis of the slit aligned along constant azimuth (i.e., the direction of atmospheric dispersion). Observations of image B were obtained only under the best seeing conditions; the seeing as estimated from examination of the images on the television guider monitor was at all times better than 0".7 (FWHM). Furthermore, in order to monitor the contamination from image A, observations were periodically taken at a position at the same elevation as that of image B, on the opposite side of the line of constant azimuth that intersected image A. *In no case was the contamination from image A found to be more than about* 5% *of the signal from image B.*

TABLE 1

LOG OF OBSERVATIONS

UM 673 Image	UT Date	Exposure Time (s)	Wavelength Coverage (Å)	Resolution (FWHM) (Å)
		MMT		
A.........	1987 Dec 11	7200	3300–4200	1
A.........	1988 Nov 10	600	3200–4800	2
A.........	1988 Nov 11	1200	3200–4800	2
B.........	1988 Nov 7	3600	3200–4800	2
B.........	1988 Nov 10	2400	3200–4800	2
B.........	1988 Nov 11	1200	3200–4800	2
		CTIO 4 m Telescope		
A.........	1988 Nov 8	3600	3800–4700	0.33
A.........	1988 Nov 8	7200	3800–4700	0.33
A.........	1988 Nov 8	7200	3800–4700	0.33
A.........	1988 Nov 9	3600	3800–4700	0.33
A.........	1988 Nov 9	2268	3800–4700	0.33
A.........	1988 Nov 10	6000	3800–4700	0.33
A.........	1988 Nov 10	5400	3800–4700	0.33
B.........	1988 Nov 9	9000	3800–4700[a]	0.33
		ESO 3.6 m Telescope		
A.........	1987 Sep 3	4800	4000–5000	0.6
A.........	1987 Sep 3	4800	4000–5000	0.6
A.........	1987 Dec 3	2700	5000–6000	1

[a] Because the poor signal-to-noise ratio, only a 200 Å interval has been illustrated in Fig. 2.

Data reductions followed standard procedures. The spectrograph is a two-channel device, allowing nearly simultaneous sky subtraction. Neither extinction correction nor flux calibration was carried out. Therefore, the spectra were reduced to units of photons pixel^{-1} s^{-1} versus heliocentric wavelengths. Since the detector is a photon counter, the variance of each spectrum was calculated on a pixel-to-pixel basis assuming that all noise resulted from photon noise in the object, sky, and dark signal. Individual spectra covering the same wavelength regions were then combined, weighted by the inverses of their corresponding variances.

The 1 Å spectrum (A image only) was calibrated with He-Ar spectra. The residuals to the fits were 0.18 Å in both spectrograph apertures. Shortward of 3500 Å, though, where there is a dearth of He-Ar lines, they were somewhat worse, perhaps twice as large. The 2 Å spectra were calibrated with He-Ar and Hg-Cd spectra, which give a larger number of lines at shorter wavelengths. The residuals to the fits were found to be 0.4 Å or less.

2.2. *The* 0.6 Å *Resolution Spectrum*

We have also used two CASPEC spectra of the A image obtained by P. M. at the coudé focus of the ESO 3.6 m telescope at La Silla. The detector was an RCA CCD, with a pixel size of 30 μm; the readout noise had been reduced by using a binning of 2 × 2 pixels during the reading. The grism had 36.1 lines mm^{-1} and the central wavelength was 4500 Å. A white internal lamp has been used for the flat field, while exposures of a thorium lamp immediately before and after the object observations were made for the calibration in wavelength. To calibrate the spectra in flux, exposures of the standard star HD 19445 were taken immediately afterward. The resolution is about 0.6 Å. The reduction followed the standard procedure described in MIDAS (Banse et al. 1988). The two spectra were then added. The spectrum has been rebinned to vacuum heliocentric wavelengths. A rough estimate of the noise has been calculated using the difference between these two spectra. Unfortunately, it was not possible to correct properly for the blaze function at the shortest wavelengths, affecting particularly a region between 4055 and 4070 Å.

2.3. *The* 0.33 Å *Resolution Spectra*

The last spectra covering the Lyα forest were obtained by R. J. W. and R. E. W. at the Ritchey-Chrétien focus of the 4 m telescope at Cerro Tololo with the echelle spectrograph. Refer to Table 1 for the log book of these observations. The detector was the CCD TI #1 with a pixel size of 15 μm; a preflash of 20 ADU over the bias was used; a binning by 2 in the direction perpendicular to the dispersion was introduced for the readout. The central wavelength was 4000 Å, with an echelle grating of 79 lines mm^{-1}; all the observations were made through a $CuSO_4$ filter. This setting introduced three major complications: first, consecutive orders do not overlap, so that gaps of several angstroms appear in the spectrum; second, there results a field curvature, introducing a variable point-spread function depending on the position in the frame; last, the difficulty of defining properly the center of the calibration lines affected the wavelength calibration, whose rms is about 0.03 Å. Due to the relatively low signal-to-noise ratio of each frame, we had to use slightly modified MIDAS reduction procedures. We extracted the spectrum with an improved routine, kindly provided to us by W. Verschueren (Verschueren & Hensberge 1990) and slightly modified in order to take into account the sky background. The latter was estimated by constructing a sky spectrum which was the average of 6 pixels, i.e., 3 pixels on both sides of each order of the object spectrum; a median filter with a window of 41 pixels was then applied on each order of this spectrum. An estimate of the variance on every pixel of each (object) spectrum was obtained by computing the difference between itself and its two closest neighbors. Comparison with an estimate of the noise on the red wing of the Lyα emission line shows good agreement. The different spectra were then co-added, weighted by the inverses of their corresponding variances.

Only the 200 Å of the B image spectrum for which the signal-to-noise ratio is the best are presented. A Gaussian filter with σ equal to the effective resolution of the instrument was applied. Because of the poor quality of these data, they were not used for the subsequent analysis. However, the reader should compare the absorption-line profiles in this spectrum with the ones in the corresponding spectrum of image A.

2.4. *The* 5000–6000 Å *Spectrum*

Finally, a spectrum of the A image covering the region from 5000 to 6000 Å was taken by P. M. with CASPEC at the ESO 3.6 m telescope in La Silla. The detector was the RCA CCD #3. A binning of 2 × 2 was applied at the reading to reduce the readout noise. The central wavelength was 5500 Å. The wavelength calibration was made using a thorium lamp and leads to an rms of 0.3 Å. Using the calibration lines, the resolution is measured to be about 1 Å. The reduction procedure followed the standard MIDAS one, except that the order extraction method was similar to the one described for the 0.33 Å spectra. Since the data were not corrected for the instrumental response, we were not able to measure the exact positions of the emission-line peaks.

3. LINE LISTS

3.1. *The* 2 Å *Resolution Spectra*

Figures 1 and 2 show the spectra of the UM 673 A and B images and their difference, illustrating their remarkable similarities. Except for a scale factor, we were able to use the same continuum for both 2 Å resolution spectra (hereafter, "2 Å spectra") obtained by fitting a fifth-order polynomial. The profiles of the emission lines (O VI, Lyα, N V) have been fitted with Gaussians. The original spectra were then normalized.

Line lists were first made by visual inspection. Positions of the absorption lines were obtained by fitting the lines with Gaussian profiles—a good approximation for the point-spread function—since lines are not resolved at this resolution; obvious blends in these spectra were fitted by multiple Gaussians (up to 3). As we analyzed the two spectra similarly and independently, the higher resolution spectra were not used for any constraints. Formal errors on the equivalent widths W were obtained using the variance spectra. Lines were accepted if their equivalent widths were at least 5 $\sigma(W)$. The line lists are presented in Table 2.

As a first result, all the 68 lines which are detected at the 5 σ level in image B are present in image A. Because of the difference in signal-to-noise ratios, the opposite is not true. However, a great number of the B lines missing at the 5 σ level are present at the 3 σ level: they are indicated in parentheses in Table 2. If they are not detected at the 3 σ level, we give the value of the 3 σ upper limit to the equivalent width of these "missing" lines.

The difference spectrum $A(2\,Å) - B(2\,Å)$ is very flat, although it exhibits some systematic differences: between 3240 and 3550 Å, the mean values measured on 10 Å spectral ranges are of the

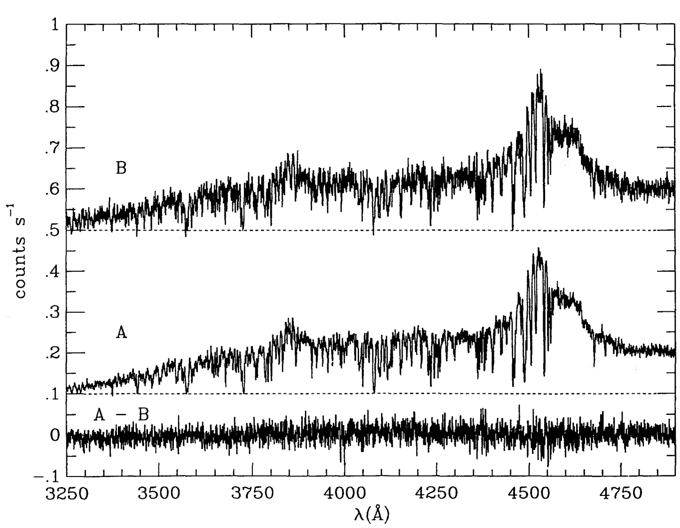

FIG. 1.—2 Å resolution spectra of the A and B images of UM 673, and their difference. Wavelengths are vacuum heliocentric. For the presentation, the spectrum of image B has been multiplied by 7.9 and offset by 0.5, and that of image A has been offset by 0.1.

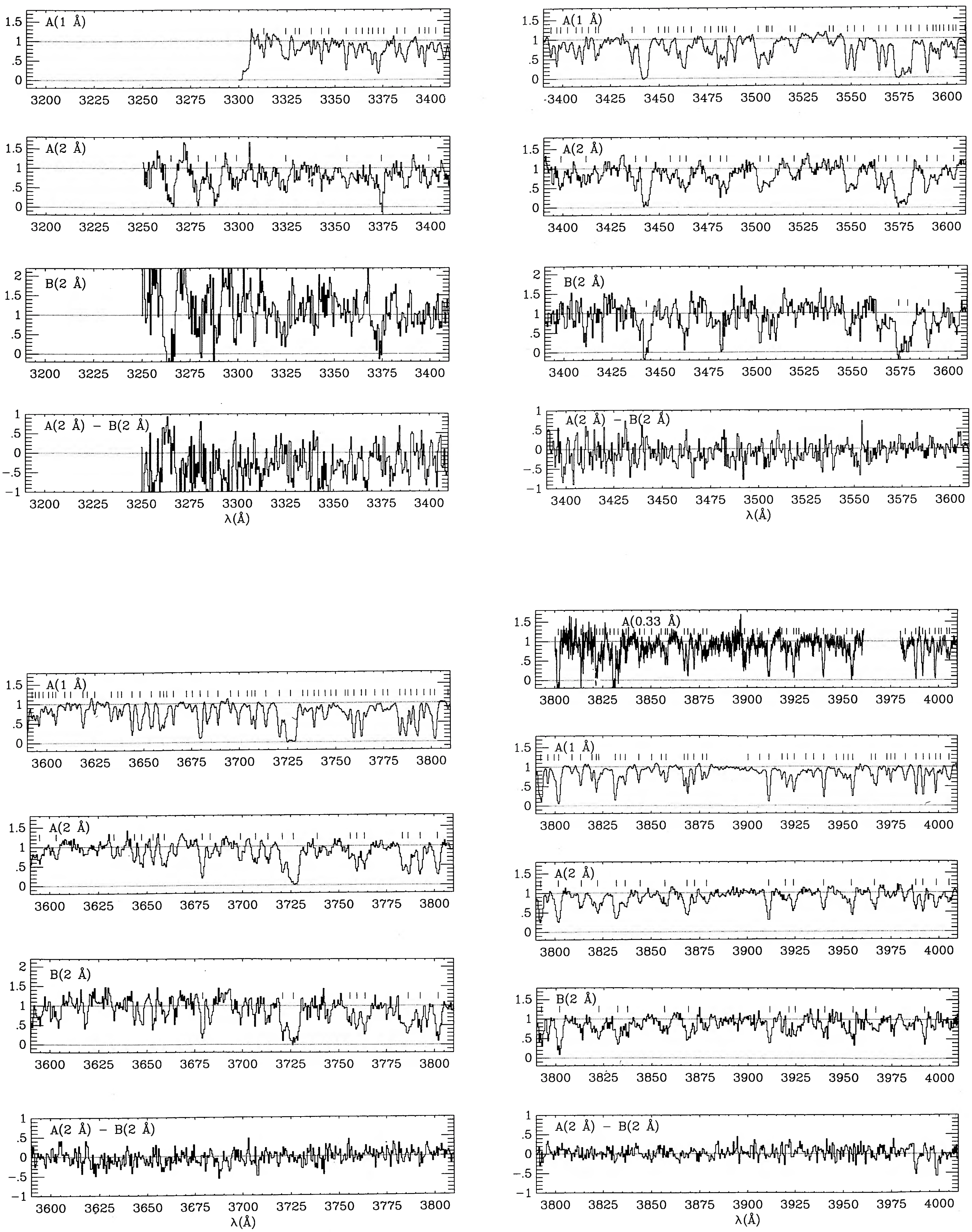

FIG. 2*a*

FIG. 2.—(*a*) Extended 2 Å spectra of the A and B images of UM 673 and the difference between the normalized spectra. For comparison the 1 Å, 0.6 Å, and 0.33 Å spectra of UM 673 image A are also shown. Wavelengths are vacuum heliocentric. Lines detected at the 5 σ level are indicated for the 2 Å, 1 Å, and 0.33 Å spectra, and at the 4 σ level for the 0.6 Å spectrum. (*b*) The C IV doublet in the 5000–6000 Å spectrum.

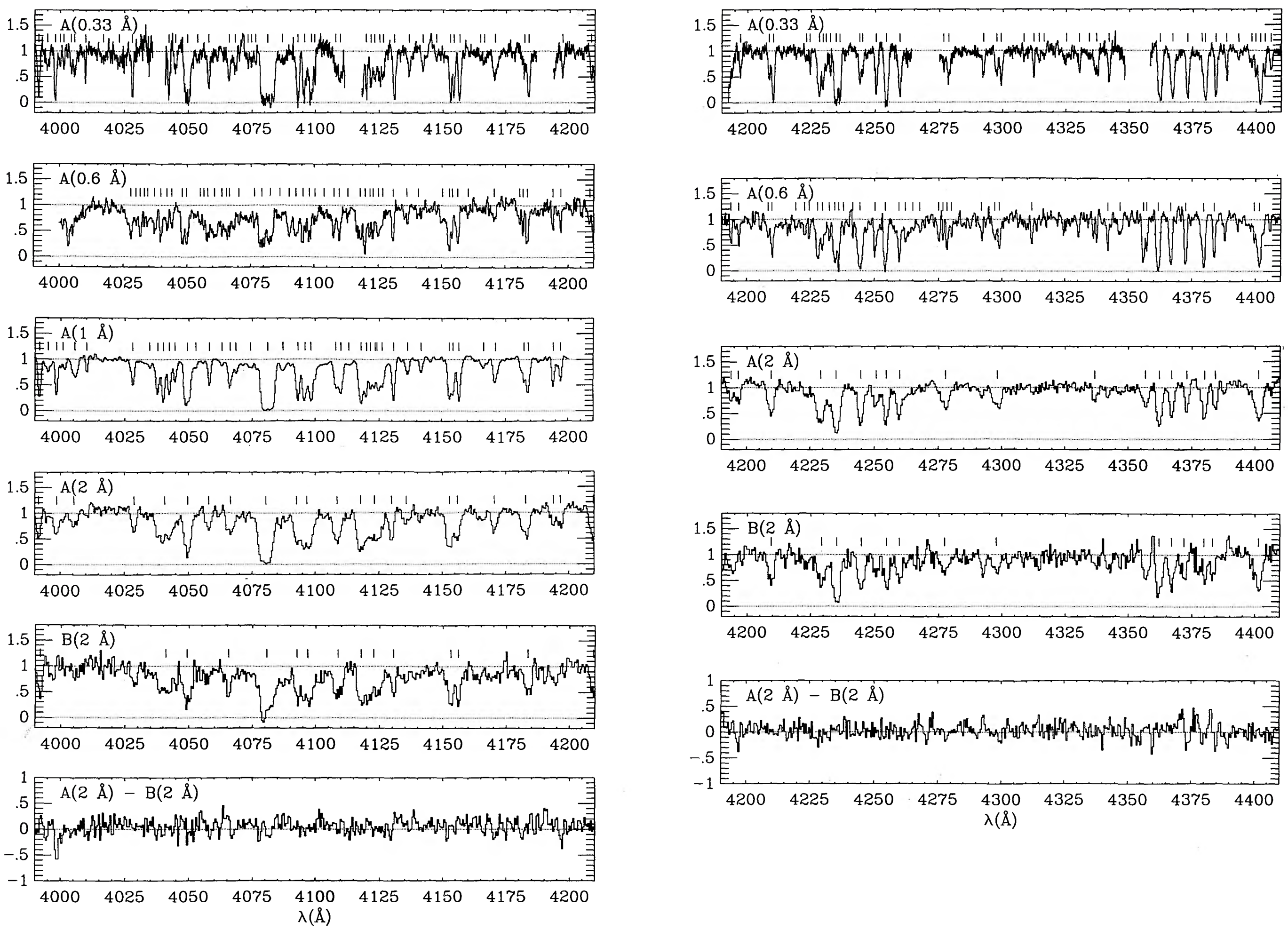

FIG. 2*a*—*Continued*

order of 0.1, with a standard deviation of 0.3, while between 4010 and 4200 Å the mean values are of the order of 0.06 and the standard deviation is of the order of 0.12. The flatness of the difference spectrum means that not only has the continuum been reasonably well fitted, but also it is nearly identical in the two spectra (at least in this spectral range). Any features in the difference spectrum are good indicators of variations between corresponding lines in the A and B spectra. They can be due to bad pixels in one or both of the spectra, differences in velocities between the two involved lines, or differences between equivalent widths. First, we define a coincidence as a line which is detected at the 5 σ level in both A and B spectra. On the other hand, since we are interested only in differences in equivalent widths, we call an anticoincidence a line which is detected at the 5 σ level in one spectrum, which is not detected at the 3 σ level in the other, and for which a feature is detected at the 3 σ level in the difference spectrum. We obtain 68 coincidences and two anticoincidences (at 3987 and 3998 Å, with 3.3 and 4.4 confidence levels respectively). The signal appearing between 4350 and 4400 Å is attributed to some "bad" pixels in the B spectrum and to a difference in velocity between two corresponding lines (cf. §§ 4.1 and 4.3.1).

3.2. *The* 0.33, 0.6, 1 Å *Resolution and* 5000–6000 Å *Spectra*

The line lists for the 0.6 and 1 Å spectra have been obtained in exactly the same way. In exceptional cases, fittings of multiple Gaussians were made with up to six components for the 0.6 Å spectrum and up to four for the 0.33 and 1 Å spectra. For the 0.6 Å spectrum, lines detected down to the 4 σ level are presented.

The positions of the components of the double C IV doublet in the 5000–6000 Å spectral range were obtained by fitting the four lines together. The relative positions and widths of the lines of the same doublet were kept fixed. The results are given in Table 4G.

Figure 2*a* presents the normalized spectra of the Lyα forest with the identified lines. Figure 2*b* displays the C IV doublet detected in the 5000–6000 Å spectrum.

4. ANALYSIS OF THE LYMAN-ALPHA LINES

4.1. *Selection of the Lyman-Alpha Lines in the* 2 Å *Spectra*

Among the 2 Å resolution spectral lines (hereafter "2 Å lines") we discriminated between lines which form blends (called hereafter "blended lines," indicated by a B in the first column of Table 2) and the lines which remain single (called "single lines," indicated by an S) when compared with the higher resolution (1, 0.6, or 0.33 Å) spectra.

Heavy-element systems were found at $z = 1.9406$, 1.9417, 1.9436, 1.9441, 2.3556, and 2.3566 (SBS; Paper II; this work),

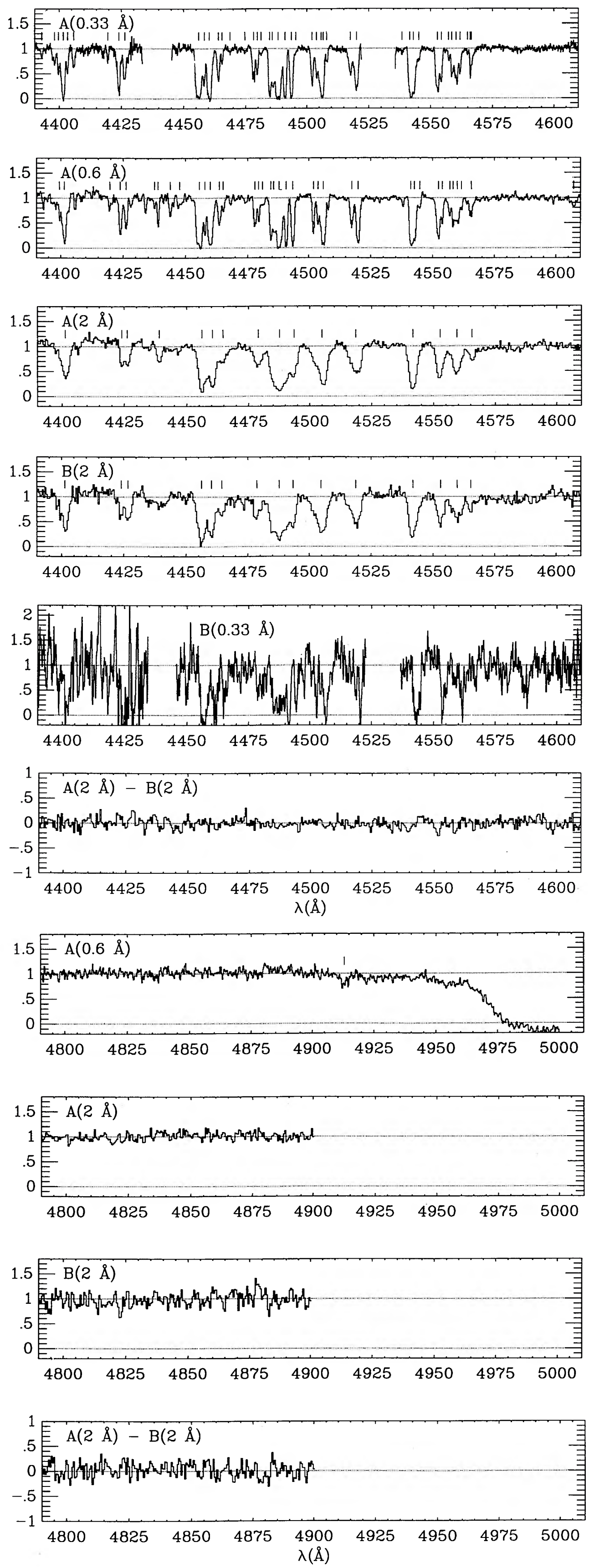

FIG. 2*a*—*Continued*

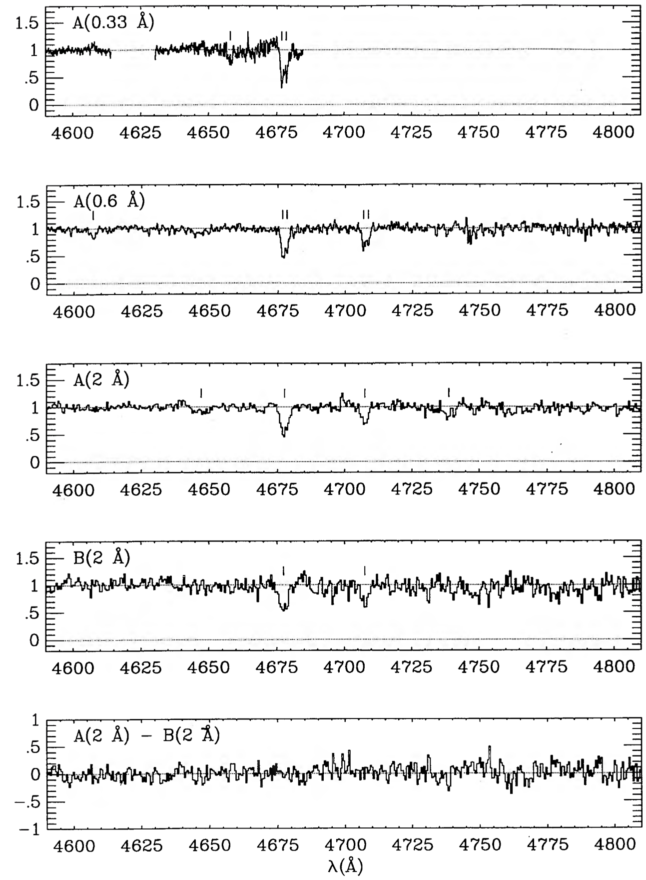

FIG. 2*a*—*Continued*

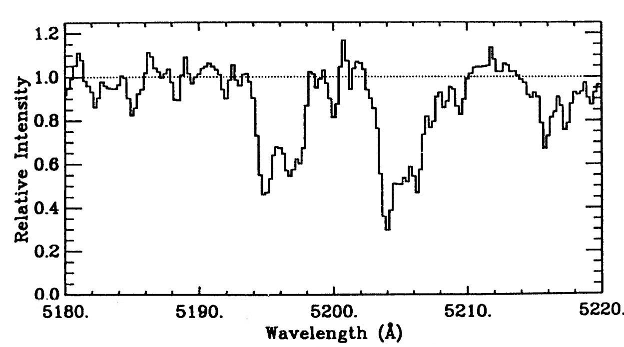

FIG. 2*b*

TABLE 2

Line Lists for 0.33, 0.6, 1, and 2 Å Resolution Spectra

			B (2Å)						A (2Å)				A (1Å)				
	1	2	λ	Wobs	σ	S/N	Δ	σ	λ	Wobs	σ	S/N	λ	σ	Wobs	σ	S/N
1		M	(3264.02	6.18	1.70	3.6)			3264.66	3.83	0.51	7.60					
2		M		4.22					3279.00	3.42	0.46	7.40					
3				4.35					3287.94	3.90	0.45	8.70					
4				4.09					3298.71	2.16	0.43	5.10					
5													3313.07	0.10	0.35	0.05	7.10
6	S			2.52					3324.33	1.87	0.36	5.30	3324.33	0.13	1.80	0.11	17.10
7													3329.25	0.07	0.40	0.05	8.00
8													3331.43	0.22	0.73	0.12	6.00
9													3337.69	0.04	0.42	0.07	6.00
10													3342.93	0.04	0.84	0.07	11.90
11													3346.63	0.08	0.43	0.09	5.00
12	S			2.18					3356.08	1.68	0.28	6.00	3355.86	0.01	1.23	0.07	18.30
13													3361.00	0.04	0.99	0.07	13.50
14													3364.20	0.06	0.38	0.06	6.90
15													3367.39	0.11	0.40	0.04	9.90
16													3369.52	0.04	1.12	0.05	24.00
17	B		(3372.93	3.65	1.05	3.5)			3374.02	3.02	0.25	12.10	3372.58	0.05	1.94	0.06	33.80
18													3375.42	0.15	0.85	0.07	12.30
19													3382.32	0.09	0.69	0.06	11.00
20													3386.43	0.06	1.82	0.07	24.30
21													3393.97	0.03	0.65	0.05	12.50
22													3396.94	0.05	1.06	0.05	20.40
23	B	L		1.56					3398.93	1.39	0.19	7.30	3398.94	0.05	0.34	0.05	7.30
24													3402.58	0.06	0.77	0.06	13.20
25													3407.02	0.02	1.17	0.05	21.50
26	B	L	(3411.04	1.33	0.41	3.2)			3411.91	0.79	0.15	5.10	3410.18	0.05	1.10	0.06	20.00
27													3413.58	0.06	0.23	0.04	5.70
28													3417.29	0.08	0.42	0.03	13.50
29													3418.74	0.38	1.04	0.08	12.70
30	S			1.67					3437.61	1.47	0.20	7.30	3436.19	0.05	1.35	0.06	23.30
31	S	M	3442.79	4.08	0.48	8.50	2.70	12.90	3443.11	4.45	0.20	22.60	3442.32	0.07	4.94	0.06	81.30
32													3449.79	0.06	0.23	0.05	5.20
33													3452.97	0.05	0.34	0.03	11.00
34	B	L		1.61					3455.70	1.05	0.20	5.30	3454.81	0.06	0.85	0.05	15.80
35	S	L	(3462.66	2.14	0.48	4.5)			3460.59	0.81	0.14	5.60	3459.65	0.04	0.59	0.02	24.90
36	B	M		1.25					3463.78	2.00	0.26	7.80	3462.65	0.04	2.55	0.06	44.70
37													3466.64	0.09	0.44	0.03	13.30
38													3473.74	0.09	0.48	0.03	14.00
39	B	M		1.36					3476.17	1.43	0.19	7.60	3476.76	0.11	1.34	0.07	19.30
40													3480.72	0.03	1.11	0.03	35.60
41	B	M	(3481.49	1.56	0.38	4.1)			3481.45	1.29	0.15	8.80	3482.85	0.04	1.19	0.05	25.80
42	B	M		0.99					3484.66	1.70	0.20	8.50	3484.70	0.03	0.80	0.03	30.20
43													3489.08	0.01	0.85	0.04	21.40
44	S		(3501.75	1.43	0.36	4.0)			3502.13	1.45	0.14	10.60	3501.30	0.06	1.46	0.03	43.40
45													3505.54	0.51	2.95	0.09	32.90
46	B		(3506.85	0.93	0.29	3.2)			3506.70	2.56	0.32	8.10	3506.46	0.08	0.32	0.02	18.60
47													3508.57	0.07	0.28	0.01	19.90
48													3518.31	0.04	0.17	0.02	7.60
49	B			1.22					3520.13	0.96	0.17	5.50	3520.73	0.03	0.99	0.06	17.20
50													3538.77	0.04	0.15	0.02	6.80
51													3540.73	0.05	0.35	0.04	8.10
52	S	M	(3547.84	1.69	0.42	4.0)			3548.10	1.64	0.16	10.30	3548.17	0.05	1.91	0.04	48.40
53	S	M		0.83					3551.73	1.76	0.19	9.10	3551.79	0.05	1.67	0.04	43.90
54													3556.49	0.06	0.44	0.03	12.70
55	S	L	(3564.27	1.68	0.37	4.5)			3564.13	1.22	0.12	9.70	3564.50	0.03	1.51	0.04	42.30
56	S	L	(3568.38	0.86	0.27	3.1)			3567.82	1.80	0.16	11.40	3568.05	0.06	1.71	0.04	44.80
57	B	M	3574.06	3.63	0.34	10.80	8.80	15.90	3574.24	3.77	0.16	24.10	3574.05	0.15	3.91	0.04	106.60
58	B	M	3578.79	4.97	0.53	9.40	-3.10	17.10	3578.89	4.25	0.18	23.80	3578.55	0.19	4.38	0.05	95.90
59													3581.12	0.06	0.66	0.01	54.00
60													3585.50	0.05	0.35	0.03	11.30
61	S		3589.70	2.20	0.33	6.80	-1.40	27.70	3589.36	1.90	0.13	14.40	3589.61	0.03	2.10	0.04	57.00
62													3592.63	0.11	0.58	0.03	20.00
63	B	L	(3594.62	1.20	0.33	3.6)			3594.89	1.06	0.13	7.90	3594.31	0.08	0.53	0.02	22.60
64													3596.12	0.05	0.83	0.03	30.50
65													3598.25	0.08	0.30	0.03	10.30
66													3601.01	0.04	0.50	0.03	14.40
67	B	L	(3604.34	1.19	0.29	4.2)			3603.46	0.70	0.13	5.50	3603.15	0.04	0.36	0.03	13.60
68													3604.77	0.02	0.74	0.03	24.70
69													3609.45	0.18	0.21	0.03	6.20
70													3612.49	0.01	0.13	0.02	5.80
71													3618.87	0.02	0.96	0.03	31.30
72													3621.08	0.12	0.32	0.05	6.80
73													3624.81	0.07	0.24	0.03	8.20
74	S	L		0.86					3633.00	0.62	0.12	5.10	3633.41	0.05	0.76	0.03	22.90
75													3636.75	0.04	0.51	0.03	16.70

TABLE 2—*Continued*

			B (2Å)						A (2Å)				A(1Å)					A(0.3Å)				
	1	2	λ	Wobs	σ	S/N	Δ	σ	λ	Wobs	σ	S/N	λ	σ	Wobs	σ	S/N	λ	σ	Wobs	σ	S/N
76													3638.69	0.03	0.48	0.03	14.50					
77	S			0.76					3643.61	0.78	0.11	7.30	3644.01	0.01	1.16	0.03	37.40					
78	S		(3647.21	1.08	0.26	4.1)			3647.34	1.15	0.13	8.90	3648.17	0.06	1.97	0.04	47.40					
79	S		(3653.47	0.81	0.26	3.1)			3653.27	0.75	0.12	6.40	3654.05	0.06	1.37	0.04	36.90					
80													3658.55	0.08	1.12	0.02	45.20					
81	B		(3659.94	0.85	0.29	3.0)			3659.19	1.81	0.15	12.10	3660.40	0.07	1.18	0.03	39.90					
82													3662.08	0.15	0.32	0.02	16.50					
83													3665.53	0.02	0.73	0.03	22.50					
84													3672.41	0.05	0.23	0.03	7.70					
85													3675.60	0.07	0.38	0.03	11.80					
86	S		3679.12	1.48	0.23	6.40	-0.60	7.10	3679.06	1.92	0.11	17.60	3679.70	0.05	2.32	0.03	74.20					
87	S		(3683.21	0.89	0.22	4.0)			3683.27	0.75	0.13	6.00	3683.72	0.08	1.09	0.03	31.60					
88													3688.91	0.02	0.69	0.03	23.90					
89													3695.50	0.04	0.27	0.03	9.40					
90	S	L		0.84					3698.97	0.93	0.12	7.50	3699.53	0.06	1.14	0.04	27.20					
91													3704.17	0.04	0.17	0.03	5.70					
92	B	M		0.87					3706.87	1.44	0.13	11.40	3706.47	0.02	0.80	0.03	29.90					
93													3708.19	0.01	0.85	0.02	36.20					
94	S	L	(3712.82	1.16	0.25	4.7)			3713.25	0.99	0.12	8.30	3713.71	0.04	1.27	0.03	37.10					
95	S		3720.88	1.53	0.18	8.70	12.20	34.90	3720.71	1.45	0.07	20.10	3720.74	0.08	1.58	0.02	89.90					
96	S		3726.36	6.06	0.50	12.20	53.60	26.50	3726.41	6.43	0.18	35.00	3726.53	0.11	7.03	0.06	124.60					
97													3732.95	0.04	0.52	0.03	18.80					
98													3735.50	0.08	0.66	0.03	20.00					
99	S			0.88					3738.75	0.75	0.13	5.70	3738.87	0.03	1.00	0.03	36.00					
100													3741.23	0.04	0.31	0.03	10.60					
101													3744.61	0.05	1.20	0.03	34.90					
102													3747.59	0.05	0.20	0.03	7.40					
103													3750.20	0.06	0.19	0.03	6.60					
104													3755.08	0.19	1.46	0.10	15.00					
105	B		3755.76	1.19	0.24	5.00	1.10	16.00	3756.11	0.60	0.09	6.90	3756.42	0.04	0.23	0.02	11.70					
106	S	L	3759.41	1.56	0.23	6.80	5.60	7.80	3759.47	1.69	0.14	12.30	3759.54	0.05	2.06	0.03	68.60					
107	B	L	3763.72	2.21	0.26	8.30	-7.30	24.10	3763.41	1.76	0.12	14.30	3763.48	0.05	1.77	0.03	64.00					
108													3765.75	0.08	0.81	0.03	27.50					
109													3770.43	0.06	0.37	0.03	13.30					
110													3774.77	0.06	0.18	0.02	9.80					
111													3777.21	0.18	0.98	0.07	13.50					
112	S		(3782.57	0.44	0.14	3.2)			3783.35	0.72	0.07	10.70	3783.63	0.02	1.65	0.03	59.50					
113	B	L	3786.28	3.78	0.46	8.20	28.70	25.50	3786.28	3.33	0.19	17.60	3786.49	0.06	2.39	0.03	93.00					
114													3789.41	0.03	0.79	0.02	34.80					
115	S		3792.53	1.60	0.21	7.50	-9.40	3.50	3792.65	1.91	0.10	18.80	3792.57	0.05	2.09	0.03	69.80					
116													3796.22	0.02	0.54	0.03	19.40					
117													3799.55	0.18	0.54	0.03	18.00					
118	B	L	3801.87	2.67	0.22	12.20	0.70	25.50	3801.71	2.23	0.11	21.10	3801.88	0.04	2.22	0.03	74.90	3801.81	0.04	2.25	0.13	16.80
119													3808.88	0.03	0.26	0.03	9.00					
120	S	L	(3813.70	0.82	0.17	4.9)			3813.74	1.04	0.11	9.80	3813.39	0.05	0.86	0.03	27.90	3813.77	0.04	0.66	0.10	6.80
121													3819.32	0.03	0.44	0.03	16.10					
122													3821.65	0.03	0.50	0.02	31.80	3821.74	0.11	1.04	0.09	11.20
123	B		3822.44	1.87	0.19	9.60	2.60	22.50	3822.24	2.35	0.14	16.60	3822.90	0.22	1.07	0.06	18.60	3823.43	0.28	0.82	0.14	5.80
124																		3825.06	0.14	0.40	0.07	5.60
125																		3828.85	0.08	0.70	0.09	7.40

TABLE 2—*Continued*

			B (2Å)						A (2Å)				A(1Å)					A(0.3Å)				
	1	2	λ	Wobs	σ	S/N	Δ	σ	λ	Wobs	σ	S/N	λ	σ	Wobs	σ	S/N	λ	σ	Wobs	σ	S/N
126	S	M	3832.39	1.84	0.19	9.90	-4.70	9.00	3832.17	2.18	0.10	22.90	3831.51	0.02	1.31	0.02	75.50	3830.96	0.05	2.06	0.10	20.20
127													3834.13	0.23	1.42	0.05	28.10	3833.01	0.11	1.57	0.15	10.60
128	B	M	3837.50	0.72	0.13	5.70	13.00	23.70	3836.75	1.22	0.10	11.70	3836.65	0.03	0.40	0.01	33.90	3837.19	0.11	0.39	0.07	6.00
129	S			0.55					3844.57	0.59	0.09	6.20	3843.67	0.04	0.64	0.03	24.10	3844.15	0.06	0.64	0.06	10.50
130																		3846.64	0.14	0.47	0.05	8.90
131													3850.22	0.03	0.25	0.02	9.90	3850.35	0.10	0.42	0.06	6.60
132													3855.21	0.08	0.38	0.02	16.70	3855.27	0.05	0.24	0.04	5.90
133	B		3856.50	1.45	0.20	7.40	59.00	27.10	3857.20	1.11	0.10	11.20	3857.62	0.03	0.73	0.02	31.80	3857.44	0.10	0.73	0.08	9.00
134																		3858.50	0.03	0.25	0.02	10.80
135													3867.12	0.03	0.71	0.02	39.10	3867.24	0.02	0.80	0.05	15.40
136	B		3868.72	1.81	0.19	9.60	6.60	8.40	3868.54	1.80	0.10	17.90	3868.92	0.02	0.98	0.02	53.00	3869.02	0.02	0.85	0.05	17.60
137	S		(3872.23	0.61	0.14	4.5)			3872.39	0.49	0.08	6.10	3872.02	0.03	0.60	0.02	26.30	3872.27	0.02	0.53	0.05	10.30
138													3876.52	0.06	0.43	0.02	19.20	3876.86	0.13	0.62	0.07	8.50
139	B		(3877.86	0.81	0.18	4.4)			3878.52	0.91	0.11	8.40	3878.61	0.05	0.63	0.03	24.10	3878.88	0.14	0.63	0.06	9.80
140																		3898.60	0.13	1.00	0.11	9.1
141													3900.23	0.04	0.26	0.03	8.20					
142													3906.37	0.04	0.59	0.03	18.00	3905.11	0.45	0.37	0.07	5.10
143	S		3911.22	1.45	0.21	7.00	0.50	5.40	3911.12	1.56	0.10	15.00	3911.16	0.02	1.75	0.03	56.40	3911.21	0.03	1.38	0.06	24.20
144													3918.18	0.08	0.56	0.03	21.00	3918.17	0.13	0.22	0.04	5.10
145	B		3921.39	1.18	0.19	6.10	1.30	28.40	3919.94	0.67	0.12	5.70	3921.01	0.08	1.22	0.03	45.00	3920.64	0.03	0.46	0.05	9.80
146	S	M	3924.61	1.05	0.17	6.10	-5.80	24.20	3924.29	1.26	0.12	10.70	3924.55	0.08	1.63	0.03	57.60	3924.34	0.04	1.16	0.06	19.10
147																		3925.76	0.03	0.21	0.04	5.20
148																		3927.02	0.07	0.25	0.04	6.30
149													3930.75	0.16	0.36	0.03	13.80					
150													3934.74	0.07	0.59	0.03	19.70					

TABLE 2—*Continued*

			B (2Å)						A (2Å)				A(1Å)					A(0.6Å)					A(0.3Å)				
	1	2	λ	Wobs	σ	S/N	Δ	σ	λ	Wobs	σ	S/N	λ	σ	Wobs	σ	S/N	λ	σ	Wobs	σ	S/N	λ	σ	Wobs	σ	S/N
151	S		3940.05	1.25	0.21	5.80	9.30	7.50	3939.95	0.97	0.10	9.50	3940.19	0.04	1.42	0.03	43.80										
152													3946.71	0.03	0.37	0.03	14.60						3946.40	0.03	0.26	0.05	5.60
153													3950.33	0.23	0.80	0.04	22.20										
154													3952.83	0.12	0.52	0.02	24.80						3952.09	0.11	0.60	0.07	8.60
155	S		3954.79	1.28	0.19	6.70	32.30	27.50	3954.47	1.61	0.12	13.50	3955.21	0.03	1.26	0.02	66.00						3954.88	0.05	1.42	0.09	16.10
156													3964.72	0.12	0.32	0.02	16.00										
157	B		3966.68	1.11	0.22	5.10	10.10	11.70	3966.45	1.18	0.11	10.60	3966.95	0.06	1.08	0.03	37.10										
158													3972.83	0.02	0.25	0.02	12.10										
159													3974.95	0.01	0.51	0.02	24.10										
160													3977.06	0.05	0.22	0.03	8.40										
161													3982.53	0.02	0.77	0.03	24.10						3982.55	0.07	0.74	0.05	14.20
162	S			0.59					3987.93	0.83	0.09	8.80	3988.17	0.02	1.02	0.03	37.50						3988.09	0.03	1.00	0.05	19.40
163	S		3991.91	1.15	0.20	5.90	-9.00	3.70	3991.56	0.95	0.09	11.00	3991.82	0.01	1.05	0.02	43.80						3991.60	0.02	0.84	0.04	18.60
164													3995.11	0.07	0.53	0.03	19.70						3995.18	0.07	0.52	0.05	10.70
165	B			0.71					3998.66	1.22	0.12	10.60	3998.42	0.03	0.82	0.02	48.80						3998.16	0.02	0.95	0.04	22.90
166																							4000.03	0.04	0.25	0.03	8.50
167													4000.93	0.23	0.48	0.04	11.80						4001.45	0.04	0.21	0.03	7.70
168																							4004.32	0.05	0.24	0.02	10.50
169	B	M		0.65					4005.40	0.74	0.11	6.80	4005.51	0.05	0.83	0.03	27.10						4005.62	0.09	0.73	0.05	13.30
170													4010.19	0.06	0.17	0.02	8.50						4009.92	0.01	0.25	0.03	8.70
171																							4016.85	0.13	0.37	0.04	8.20
172																							4022.97	0.17	0.60	0.06	9.70
173	S	M	(4028.63	0.90	0.20	4.6)			4028.70	0.70	0.09	8.00	4028.09	0.03	0.79	0.03	30.90	4027.89	0.09	1.03	0.13	8.10	4028.09	0.02	0.83	0.07	12.30
174																		4029.86	0.06	0.46	0.08	5.80					
175																		4031.55	0.02	0.80	0.09	8.50					
176																		4033.16	0.07	0.30	0.05	6.60					
177													4034.68	0.12	0.36	0.03	14.30	4034.41	0.07	0.54	0.09	6.20					
178													4037.85	0.05	1.28	0.02	57.00	4037.17	0.06	0.93	0.08	12.30					
179	B		4040.98	3.58	0.29	12.40	-23.90	31.10	4040.74	3.87	0.15	25.50	4040.05	0.03	1.44	0.02	78.20	4039.69	0.06	0.98	0.07	13.90					
180													4042.35	0.03	1.14	0.02	56.70	4042.02	0.06	0.68	0.07	9.70	4042.41	0.03	0.74	0.07	11.10
181													4044.57	0.03	0.68	0.02	28.70	4043.93	0.04	0.49	0.06	8.40	4044.97	0.05	0.39	0.05	7.20
182																		4048.05	0.06	0.85	0.05	17.60					
183	B+	M	4049.27	2.70	0.28	9.80	2.10	27.20	4049.65	2.52	0.11	22.40	4049.39	0.05	2.75	0.04	76.70	4049.79	0.09	1.53	0.08	18.70	4049.64	0.05	2.63	0.06	42.20
184													4052.75	0.25	0.23	0.02	12.00						4053.68	0.09	0.24	0.03	6.80
185	S			0.57					4057.92	0.73	0.09	7.90	4058.08	0.02	0.67	0.03	25.50	4058.00	0.07	1.12	0.05	22.00	4058.08	0.03	0.87	0.04	20.40
186																		4060.65	0.09	1.75	0.07	24.50					
187													4063.05	0.04	0.19	0.02	8.50	4063.55	0.02	0.54	0.03	17.90					
188																		4065.32	0.15	1.09	0.05	22.50					
189	B		4065.49	1.30	0.18	7.10	41.00	65.40	4066.50	1.31	0.10	12.80	4066.24	0.05	1.07	0.03	42.40	4066.59	0.05	0.53	0.04	13.20	4066.02	0.04	0.75	0.04	20.70
190													4068.50	0.09	0.53	0.02	22.50						4068.32	0.06	0.47	0.03	15.40
191																		4070.27	0.04	0.40	0.08	4.80					
192																							4073.39	0.04	0.25	0.03	8.10
193													4074.28	0.09	0.47	0.03	17.30						4074.77	0.07	0.30	0.03	10.00
194																		4076.37	0.06	0.49	0.04	11.50	4076.35	0.04	0.21	0.02	9.00
195																		4079.22	0.14	2.40	0.15	16.50					
196	B+	M	4080.62	6.60	0.29	22.90	21.00	4.40	4080.46	6.43	0.12	52.30	4081.14	0.11	6.31	0.03	183.30	4082.55	0.15	1.82	0.13	14.40	4081.16	0.09	5.76	0.06	97.90
197													4087.27	0.04	0.61	0.03	21.70	4086.34	0.33	0.52	0.09	6.10	4086.97	0.13	0.62	0.04	15.10
198																		4090.07	0.02	1.19	0.07	16.20					
199	B		4092.56	1.23	0.17	7.20	37.90	32.60	4092.59	1.28	0.09	15.00	4093.20	0.03	1.56	0.02	66.70	4092.78	0.04	1.36	0.08	16.60	4093.05	0.02	1.44	0.05	27.20
200	B	M	4096.78	3.84	0.39	9.80	?		4096.69	3.79	0.16	23.40	4095.95	0.10	1.87	0.02	101.90	4095.57	0.09	1.44	0.11	12.70	4095.66	0.04	1.38	0.05	28.90

TABLE 2—*Continued*

			B (2Å)						A (2Å)				A(1Å)					A(0.6Å)					A(0.3Å)				
	1	2	λ	Wobs	σ	S/N	Δ	σ	λ	Wobs	σ	S/N	λ	σ	Wobs	σ	S/N	λ	σ	Wobs	σ	S/N	λ	σ	Wobs	σ	S/N
201													4098.30	0.12	2.12	0.03	81.00	4098.05	0.07	1.09	0.08	13.40	4098.21	0.05	1.73	0.05	35.20
202																		4100.27	0.11	0.66	0.07	9.60	4099.67	0.04	0.40	0.04	9.90
203																		4103.88	0.09	0.32	0.07	4.30					
204													4107.96	0.05	0.95	0.02	41.90	4107.62	0.05	0.89	0.06	15.10	4107.83	0.22	0.52	0.07	7.20
205	B		4108.56	2.41	0.22	10.70	0.10	7.90	4108.59	1.94	0.10	20.00	4109.94	0.05	1.37	0.03	51.70	4109.75	0.05	1.04	0.08	13.70	4109.73	0.15	1.10	0.09	12.50
206													4113.10	0.11	0.29	0.03	11.20	4113.13	0.12	0.29	0.04	7.40					
207	B		4117.70	1.96	0.23	8.52	-1.30	15.40	4117.78	2.30	0.10	23.80	4117.85	0.04	1.86	0.03	69.40	4117.86	0.12	1.62	0.08	19.40					
208													4119.96	0.04	1.10	0.02	52.50	4119.82	0.05	1.34	0.04	33.10	4119.88	0.04	0.86	0.05	17.60
209													4121.53	0.24	1.22	0.05	26.10	4121.68	0.03	0.60	0.02	27.10	4121.69	0.05	0.72	0.03	26.70
210	B	M	4122.59	4.13	0.47	8.81	44.80	54.90	4123.17	3.68	0.19	19.50	4123.40	0.11	0.47	0.03	18.60	4122.86	0.04	0.73	0.03	29.20	4123.20	0.06	0.76	0.03	22.50
211													4124.10	0.42	0.82	0.03	29.00	4124.91	0.06	1.22	0.10	12.20	4125.10	0.08	0.91	0.04	23.50
212													4126.03	0.69	1.28	0.04	34.90	4126.54	0.05	0.26	0.05	5.40	4126.53	0.09	0.52	0.03	19.00
213	S		4130.36	1.23	0.18	6.80	-8.00	15.90	4129.81	1.16	0.09	12.30	4130.64	0.02	1.27	0.02	53.00	4130.65	0.04	0.85	0.10	8.70	4130.84	0.01	1.16	0.03	34.00
214	S			0.63					4135.60	0.53	0.11	5.00	4136.14	0.02	0.47	0.03	16.90	4136.11	0.10	0.60	0.10	5.90	4136.59	0.04	0.63	0.03	18.10
215													4141.69	0.05	0.33	0.03	12.40	4140.67	0.11	0.26	0.04	6.50	4142.01	0.03	0.39	0.02	17.30
216																							4147.36	0.04	0.13	0.02	6.00
217																		4150.15	0.11	0.59	0.03	19.80					
218	B		4153.01	2.24	0.19	11.90	0.30	27.90	4152.72	2.10	0.10	20.40	4152.82	0.01	0.94	0.02	50.30	4152.91	0.07	1.86	0.13	14.20	4152.87	0.02	1.20	0.03	41.70
219													4154.34	0.02	1.18	0.02	49.50	4154.11	0.06	0.09	0.02	4.90	4154.29	0.02	0.87	0.02	37.20
220	S		4155.96	1.89	0.21	9.10	-14.10	24.80	4155.90	1.25	0.09	14.60	4156.68	0.04	1.36	0.03	52.60	4156.24	0.06	1.17	0.05	23.50	4156.55	0.01	1.19	0.03	38.70
221																		4160.32	0.08	0.22	0.04	5.10					
222																							4164.79	0.07	0.15	0.02	6.20
223													4166.23	0.11	0.36	0.03	12.60						4166.38	0.09	0.32	0.03	11.00
224	S			0.69					4170.34	0.90	0.11	8.20	4170.86	0.04	0.92	0.03	31.20	4170.58	0.09	0.48	0.09	5.40	4170.66	0.04	1.10	0.04	26.90
225																		4180.61	0.12	0.44	0.05	8.10					
226	B		4183.46	1.68	0.21	7.90	15.40	18.00	4182.77	1.57	0.11	14.00	4182.32	0.24	0.94	0.03	32.60	4181.98	0.01	0.47	0.06	8.40	4182.25	0.11	0.63	0.05	11.40
227													4184.01	0.08	0.78	0.02	46.70	4183.68	0.04	1.00	0.07	14.10	4184.00	0.03	1.06	0.04	30.40
228	S		(4194.19	0.98	0.21	4.6)			4193.86	0.40	0.07	5.70	4194.06	0.04	0.64	0.02	31.60	4193.74	0.05	0.42	0.10	4.00					
229	S			0.43					4196.61	0.65	0.11	6.00	4196.94	0.08	0.59	0.02	26.90	4196.88	0.04	0.50	0.08	5.90	4197.22	0.03	0.41	0.03	14.40
230																		4208.33	0.04	0.45	0.08	5.90	4208.57	0.02	0.55	0.02	24.70
231	B		4209.42	1.42	0.20	7.30	-0.10	4.50	4209.54	1.33	0.10	12.90						4209.89	0.03	0.91	0.08	11.40	4210.12	0.01	1.14	0.03	43.80
232																		4219.29	0.09	0.22	0.05	4.50					
233																		4222.62	0.04	0.42	0.06	7.60	4223.19	0.11	0.21	0.02	10.10
234																		4224.44	0.04	0.28	0.05	5.90	4224.59	0.01	0.23	0.02	11.50
235																		4227.71	0.08	1.17	0.10	11.30	4228.22	0.02	1.43	0.03	46.90
236	B	M	4229.34	2.13	0.19	11.10	-9.00	16.80	4229.10	2.62	0.10	26.90						4229.70	0.13	1.05	0.14	7.70	4229.76	0.02	0.63	0.02	38.00
237																							4230.96	0.05	0.37	0.02	19.70
238																		4232.30	0.07	0.41	0.06	7.00	4232.57	0.02	0.27	0.02	12.90
239																		4234.48	0.07	1.57	0.09	17.30	4234.75	0.03	2.03	0.04	48.10
240	S		4235.23	3.16	0.19	16.60	16.40	26.70	4235.02	3.44	0.11	32.50						4236.02	0.05	0.84	0.05	16.90	4236.29	0.02	0.81	0.02	38.10
241																		4237.90	0.03	0.23	0.04	5.70					
242																		4241.52	0.06	0.16	0.03	5.50					
243																							4243.96	0.04	0.66	0.03	24.40
244	B		4244.70	1.98	0.20	9.90	-3.40	9.20	4244.67	1.83	0.09	19.80						4244.32	0.02	2.33	0.12	19.70	4245.03	0.05	0.42	0.03	16.90
245	S		(4250.45	0.86	0.18	4.8)			4250.67	0.96	0.10	10.00						4250.27	0.07	0.98	0.12	7.90	4250.39	0.02	0.89	0.04	23.80
246	S		4254.54	1.53	0.17	8.90	-2.10	2.20	4254.52	1.55	0.08	19.10						4254.21	0.05	1.59	0.07	21.70	4254.25	0.02	1.78	0.04	40.20
247	B		4259.48	1.27	0.18	7.20	-11.60	3.00	4259.71	1.68	0.10	16.90						4259.58	0.04	1.08	0.12	8.80	4259.54	0.02	1.22	0.06	19.90
248																		4262.02	0.05	0.33	0.07	4.70					
249																		4264.98	0.06	0.26	0.04	6.90					
250																		4267.64	0.06	0.36	0.05	7.10					

TABLE 2—*Continued*

			B (2Å)						A (2Å)				A(0.6Å)					A(0.3Å)				
	1	2	λ	Wobs	σ	S/N	Δ	σ	λ	Wobs	σ	S/N	λ	σ	Wobs	σ	S/N	λ	σ	Wobs	σ	S/N
251													4274.95	0.04	0.47	0.09	5.40					
252													4276.67	0.05	0.26	0.06	4.10	4276.69	0.05	0.35	0.02	14.50
253	B		4277.29	1.26	0.21	5.90	16.00	21.70	4277.71	1.43	0.12	11.50	4278.23	0.05	0.57	0.04	13.60	4278.65	0.05	0.90	0.04	22.50
254													4279.95	0.05	0.29	0.03	8.60					
255													4291.78	0.09	0.41	0.07	5.60	4292.32	0.02	0.51	0.02	20.80
256													4296.94	0.06	0.59	0.06	9.50	4297.53	0.04	0.61	0.03	21.60
257	B		4297.78	1.10	0.20	5.50	27.20	15.20	4298.08	1.48	0.11	12.90	4298.72	0.03	0.71	0.06	12.40	4299.28	0.03	0.76	0.03	27.70
258																		4308.40	0.05	0.13	0.02	5.70
259													4311.85	0.03	0.38	0.04	9.20	4312.24	0.02	0.37	0.02	15.30
260																		4314.39	0.05	0.20	0.02	8.50
261																		4316.29	0.07	0.15	0.02	6.10
262																		4325.12	0.19	0.50	0.04	13.10
263																		4330.29	0.02	0.33	0.03	12.50
264																		4334.19	0.13	0.28	0.04	6.60
265	B		(4337.03	0.59	0.19	3.1)			4336.80	0.53	0.09	5.70						4337.01	0.07	0.88	0.04	21.1
266													4341.77	0.04	0.59	0.09	6.30	4341.98	0.02	0.57	0.04	12.70
267													4346.52	0.09	0.47	0.10	4.50					
268													4355.87	0.03	1.45	0.11	13.30					
269	B		(4356.98	1.11	0.23	4.8)			4356.69	0.99	0.11	8.90	4357.19	0.04	1.45	0.11	13.30					
270	S		4362.08	2.04	0.24	8.40	4.00	11.40	4362.14	1.79	0.10	18.60	4361.68	0.05	1.48	0.07	20.40	4362.09	0.03	1.76	0.03	50.20
271	S		4366.91	1.56	0.22	7.20	2.60	2.20	4366.95	1.16	0.10	11.60	4366.59	0.03	1.10	0.09	11.80	4366.93	0.02	1.80	0.03	55.20
272	S		4371.79	1.12	0.19	5.90	21.20	7.80	4372.87	0.73	0.08	8.70	4372.49	0.04	0.79	0.06	12.20	4372.90	0.01	1.25	0.03	44.90
273	B		4379.63	1.50	0.22	6.80	-2.20	7.40	4379.92	1.31	0.10	12.50	4379.52	0.04	1.37	0.09	15.60	4379.78	0.02	1.78	0.03	49.10
274	S		4383.15	0.86	0.16	5.30	12.50	21.40	4384.21	0.73	0.08	9.60	4383.70	0.03	0.58	0.09	6.20	4383.94	0.02	1.01	0.03	31.20
275																		4388.17	0.03	0.42	0.02	17.50
276																		4392.92	0.02	0.15	0.02	7.70
277																		4398.14	0.05	0.43	0.02	17.70
278													4399.49	0.08	0.28	0.02	14.60	4399.73	0.02	0.40	0.03	28.00
279	B		4401.34	2.34	0.22	10.60	5.30	11.40	4401.39	2.30	0.12	18.60	4401.43	0.07	2.33	0.07	32.80	4401.62	0.01	1.90	0.01	61.10
280																		4403.44	0.02	0.32	0.02	25.90
281																		4405.89	0.02	0.41	0.02	16.30
282													4419.70	0.11	0.27	0.03	7.90	4419.63	0.03	0.17	0.02	7.00
283	S		4424.02	0.75	0.14	5.30	24.00	19.20	4424.07	0.61	0.06	10.10	4423.89	0.02	0.96	0.05	18.10	4424.03	0.02	1.32	0.04	35.10
284	S		4426.74	1.27	0.17	7.40	6.30	6.40	4426.29	0.88	0.09	9.60	4426.11	0.03	0.76	0.06	12.10	4426.44	0.04	1.01	0.04	26.10
285													4437.57	0.03	0.19	0.03	6.30					
286	B			0.43					4439.08	0.69	0.07	9.30	4438.96	0.01	0.45	0.05	9.20					
287													4443.90	0.03	0.38	0.04	9.90					
288													4447.68	0.16	0.32	0.05	6.60					
289	B		4456.24	3.36	0.13	25.70	-0.40	29.00	4456.19	3.19	0.06	52.00	4455.68	0.04	3.09	0.07	46.80	4456.06	0.04	2.89	0.04	77.10
290													4457.86	0.04	0.34	0.02	22.40	4458.33	0.04	0.59	0.01	41.10
291	S		4460.25	2.38	0.11	21.10	10.30	7.60	4460.33	2.85	0.06	45.80	4460.02	0.04	2.40	0.05	43.70	4460.38	0.02	2.31	0.02	91.70
292													4463.67	0.01	0.74	0.04	19.90	4464.09	0.01	0.77	0.02	39.90
293	B		4464.44	1.18	0.12	9.70	-1.00	19.40	4464.70	1.18	0.07	17.30	4465.19	0.03	0.28	0.05	6.10	4465.55	0.01	0.25	0.01	17.10
294																		4468.71	0.08	0.08	0.01	5.70
295																		4474.71	0.09	0.08	0.01	6.50
296													4477.94	0.04	0.75	0.03	21.90	4478.25	0.03	0.82	0.02	36.70
297	B	M	4478.70	1.35	0.12	11.10	-5.00	7.30	4478.97	1.60	0.08	20.40	4479.44	0.03	0.50	0.03	15.10	4479.74	0.03	0.42	0.01	30.40
298													4481.03	0.19	1.43	0.08	19.10	4481.23	0.03	0.16	0.01	11.70
299													4484.44	0.04	0.89	0.02	39.70	4484.76	0.04	0.86	0.01	90.90
300													4485.62	0.08	0.47	0.02	20.30	4485.89	0.09	0.75	0.01	55.80
301	B		4487.77	6.69	0.25	26.50	-0.70	-6.30	4487.67	7.18	0.13	57.10	4487.86	0.03	3.30	0.06	51.30	4488.29	0.04	3.19	0.03	106.70
302													4490.74	0.02	1.41	0.03	44.00	4491.01	0.02	1.50	0.02	74.70
303	S		4493.46	0.91	0.07	13.40	-17.10	17.30	4493.61	1.04	0.04	25.70	4493.47	0.03	1.45	0.04	36.80	4493.64	0.01	1.59	0.02	75.20
304													4501.96	0.01	0.71	0.03	21.40	4502.09	0.01	0.85	0.02	46.80
305													4503.79	0.06	0.45	0.03	15.30	4503.89	0.04	0.60	0.01	40.10
306	B		4504.73	3.84	0.15	25.50	27.80	24.60	4504.99	3.90	0.08	48.30	4505.96	0.04	2.22	0.07	33.40	4505.71	0.10	1.73	0.02	74.30
307																		4506.69	0.03	0.49	0.01	41.30
308																		4508.09	0.03	0.27	0.01	18.30
309													4517.47	0.02	0.84	0.04	23.60	4517.58	0.03	0.85	0.02	41.50
310	B		4518.84	2.37	0.14	17.50	23.10	27.50	4518.64	2.52	0.07	34.40	4519.97	0.02	1.54	0.04	43.60	4520.01	0.02	1.44	0.02	72.00
311																		4538.40	0.05	0.10	0.01	8.80
312	B		4541.91	3.09	0.12	24.90	-0.20	5.00	4541.57	3.18	0.07	47.40	4541.05	0.07	1.12	0.04	29.90	4541.46	0.07	1.06	0.02	87.00
313													4542.52	0.10	1.62	0.05	30.90	4542.95	0.10	1.90	0.01	105.60
314													4544.74	0.09	0.20	0.03	7.40	4545.18	0.08	0.25	0.02	25.00
315	B	M	4552.97	1.69	0.13	13.50	-12.40	7.70	4552.52	2.17	0.06	34.10	4552.38	0.02	1.56	0.05	33.40	4552.79	0.03	1.50	0.02	72.10
316													4554.00	0.02	0.38	0.02	18.60	4554.32	0.03	0.54	0.01	48.70
317													4556.95	0.03	0.43	0.04	11.30	4557.30	0.04	0.18	0.01	29.00
318													4558.23	0.05	0.44	0.03	14.70	4558.55	0.03	0.53	0.01	59.70
319	B	M	4559.71	2.07	0.14	15.10	-6.50	29.20	4559.33	2.24	0.07	32.30	4559.91	0.10	1.13	0.06	17.40	4560.29	0.03	1.28	0.02	75.20
320													4561.58	0.04	0.24	0.04	5.90	4561.90	0.03	0.35	0.01	47.40
321																		4564.89	0.03	0.07	0.01	6.80
322	B	M	4565.23	0.91	0.14	6.60	13.90	16.40	4565.48	0.79	0.06	13.10	4565.61	0.08	0.56	0.07	7.60	4565.96	0.01	0.15	0.01	27.90
323																		4566.46	0.06	0.50	0.02	22.00
324																		4585.60	0.36	0.26	0.02	12.30
325													4607.14	0.10	0.39	0.09	4.10					
326				0.65					4647.06	0.65	0.12	5.50										
327																		4657.98	0.11	0.40	0.03	11.70
328													4676.78	0.10	0.94	0.05	17.60	4676.79	0.04	0.72	0.03	22.90
329	B	M	4677.40	1.67	0.22	7.70	-6.05	9.75	4677.56	1.69	0.12	14.30	4678.38	0.13	0.61	0.05	12.40	4678.37	0.06	0.72	0.04	17.30
330													4706.78	0.08	0.56	0.05	11.50					
331	B	M	4707.58	1.09	0.20	5.60	-2.00	12.60	4707.40	0.88	0.10	8.60	4708.54	0.10	0.46	0.05	9.00					
332		M		0.77					4738.69	0.72	0.13	5.40										
333													4913.06	0.19	1.01	0.15	6.90					

using mainly the higher resolution spectra and the identification list of Morton, York, & Jenkins (1988). They are presented in Table 4 and are analyzed independently (cf. § 5).

It also appears that the two reported anticoincidences at 3987 and 3998 Å are compatible with the Mg II $\lambda\lambda$2796 and 2802 doublet at a redshift $z = 0.4261$. A search for other lines at the same redshift leads to the possible identification of Mg I λ2852 at 4068 Å, but no other line was found. If we consider the two anticoincidences as due to Lyα lines, and if we take into account the fact that they are the only anticoincidences, it is a posteriori quite unexpected to find them so close to each other and with their relative positions and strengths similar to those expected for a Mg II doublet. However, this hypothesis cannot be totally excluded: the expected number of Lyα lines which fulfill these conditions within a measurement uncertainty of 0.1 Å (corresponding to an observed 10^{-4} scatter in the determination of the redshift of heavy-element systems) is about 7.5×10^{-4}. On the other hand, we could hope to detect the responsible galaxy at such a redshift. The analysis of a 30 minute R image used by Magain et al. (1990) shows a diffuse feature near the quasar: its identification as the responsible object remains in doubt, since it lies closer to B than to A, and since no spectrum had been taken yet. The galaxy D (cf. Paper I) which appears south of UM 673 is not involved, since its redshift has been measured to be 0.17 (Surdej 1990).

In the higher resolution spectra, a line is interpreted as a Lyβ line if its position relative to an already selected Lyα line, with equivalent width $W_{\mathrm{Ly}\alpha}$, is similar within the measurement uncertainty to that expected from the wavelength ratio, and if its equivalent width $W < W_{\mathrm{Ly}\alpha} + 3\sigma(W_{\mathrm{Ly}\alpha})$. We have also applied the corresponding criterion to the suspected Lyγ lines with respect to the accepted Lyβ lines.

If any line in the high-resolution spectra (including Lyα) of one of the heavy-element systems can be interpreted as a subcomponent of a blended line (in the 2 Å spectra) or is the corresponding line of a single line (in the 2 Å spectra), this (blended or single) line is marked M in Table 2 (second column) and is not considered as a possible Lyα (cloud) line; this is quite restrictive, as it may happen that the equivalent width of a heavy-element system line in the high-resolution spectra is very small compared with the corresponding blended line. The same rule was applied for the Lyβ and Lyγ lines. However, in this case, the involved 2 Å lines are indicated by an L in Table 2.

Since there remains some doubt on the reality of the anticoincidences as Lyα lines, we shall consider in what follows two distinct cases. Case 1: our sample of Lyα lines contains 47 coincidences i.e., 21 single lines and 26 blended lines, and two anticoincidences. Case 2: we have 46 coincidences, i.e., 20 single lines and 26 blended lines, and no anticoincidences.

4.2. *Diameter of Lyman-Alpha Clouds*

4.2.1. *Separations between the Light Beams*

By definition of the angular-diameter distance, the comoving linear separation $S(z_d)$ at the redshift of the lens is given by $S(z_d) = \theta D_{\mathrm{od}}$ and also by $S(z_d) = \theta' D_{\mathrm{sd}}$, where θ' is the angle between the light beams at the source position (cf. Fig. 3 for the geometry of this gravitational lens system). Simple geometrical considerations give the proper separation $S(z_i)$, for a cloud i at redshift z_i, between the light beams:[10]

$$S(z_i) = \theta \frac{D_{\mathrm{od}} D_{\mathrm{sc}}(z_i)}{D_{\mathrm{sd}}} \tag{1}$$

where θ is the angular separation between the A and B images of UM 673, D_{od} is the angular diameter distance between the observer and the deflector, $D_{\mathrm{sc}}(z_i)$ is the angular-diameter distance between the source and the cloud at redshift z_i, and D_{sd} is the angular-diameter distance between the source and the deflector.

A general formula to compute these angular-diameter distances is given in Blandford & Kochanek (1987):

$$D_{ij} = \frac{2c}{H_0} \frac{(1 - 2q_0)(G_i - G_j) + (G_i G_j^2 - G_i^2 G_j)}{(2q_0)^2(1 + z_i)(1 + z_j)^2}, \tag{2}$$

where $G_i = (1 + 2q_0 z_i)^{1/2}$.

D_{sc} and D_{sd} are related to D_{cs} and D_{ds}, respectively, by

$$D_{\mathrm{sc}} = D_{\mathrm{cs}} \frac{1 + z_s}{1 + z_c} \tag{3}$$

and

$$D_{\mathrm{sd}} = D_{\mathrm{ds}} \frac{1 + z_s}{1 + z_d}. \tag{4}$$

For UM 673 the linear separation between the light beams is represented as a function of redshift in Figure 4.

4.2.2. *Correlation of the Equivalent Widths*

Figure 5*a* plots the rest equivalent width (W_B) of Lyα lines in spectrum B versus that (W_A) for the corresponding line in spectrum A; for the 21 single lines (*solid-line symbols*) and the 26

[10] Note that, using $S(z_d) = \theta' D_{\mathrm{ds}}$, instead of $S(z_d) = \theta' D_{\mathrm{sd}}$, Foltz et al. (1984) have obtained the formula $S = \theta D_{\mathrm{od}} D_{\mathrm{cs}}(z_i)/D_{\mathrm{ds}}$, which is then wrong by a factor $(1 + z_d)/(1 + z_c)$: the published values for the separation between the light beams of images A and B of Q2345+007 at $z_a = 1.951$ should then be approximately multiplied by 0.5, 0.7, and 0.9 for $z_d = 0.5$, 1, and 1.5, respectively. Basically, the same error has been made Young et al. (1980, 1981): the separation between the light beams for the absorption systems at $z_a = 1.1249$, 1.3911 in the spectra of Q0957+561 should be approximately multiplied by 0.5 and 0.4, respectively.

NOTE.—Columns are arranged for easy comparison with the corresponding spectra. A "B" in the first column means that the lines in the 2 Å spectra are blended when comparison is made with the higher resolution spectra; otherwise an "S" is indicated. An "M" ("L") in the second column means that the line—or at least one of the subcomponents in the higher resolution spectra, if the line is blended—belongs to a metallic system (can be a Lyβ or Lyγ line). A "B+" in the first column means that the line is taken as blended most probably because of a bad sky subtraction in the 0.6 Å spectrum. For the 2 Å spectra, central wavelengths (λ), observed equivalent width (W_{obs}), formal error on the equivalent widths (σ), and signal-to-noise ($= W_{\mathrm{obs}}/\sigma$) for the absorption lines are given. Difference in velocities (Δ) and associated formal errors (σ) in kilometers per second are also given for the single and blended coincidence lines. For the other spectra central wavelengths (λ) and associated fitting errors (σ), observed equivalent widths (W_{obs}), formal error on equivalent widths (σ), and signal-to-noise ratios ($= W_{\mathrm{obs}}/\sigma$) are given. For the B image, characteristics within parentheses mean that the line is detected at only the 3 σ level. If only the equivalent width is given, the value is a 3 σ upper limit. All wavelengths are heliocentric vacuum values. Wavelengths and equivalent widths are in angstroms. (The question mark for the line at 4096 Å means that the cross-correlation function presents two peaks of nearly equal intensity corresponding to $\Delta = -70.5 \pm 15.8$ km s^{-1} and $\Delta = 40.3 \pm 23.4$ km s^{-1}.)

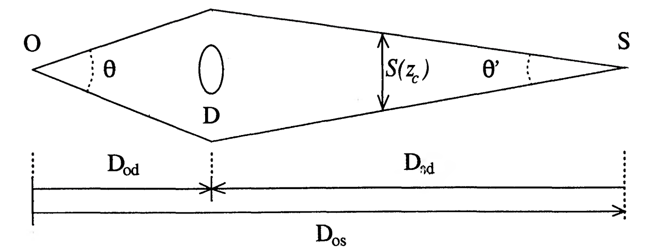

FIG. 3.—Geometry of a gravitational lens system. Symbols are defined in the text.

blended lines (*dashed-line symbols*). In all cases, the correlation is excellent. The dispersion is consistent with that expected from measurement errors alone. In particular, it is reasonable to believe that (1) the number of components among the blended lines is the same in the spectrum of B as in that of A and (2) the individual components of each blended line are also very well correlated in the two spectra. Figure 5*b* shows W_B versus W_A for the B lines detected at the level of 3 σ to 5 σ: most of them do follow the general correlation between W_A and W_B. This figure presents also the 3 σ upper limit for the rest equivalent width of the A lines which are "missing" in the B spectrum. Here also, most of them are compatible with the general correlation.

We consider that the remarkable correlation existing between W_A and W_B is a proof that both light beams actually cross the same Lyα clouds (assuming their intergalactic nature; SYBT). If small Lyα clouds were clustered, as required, for

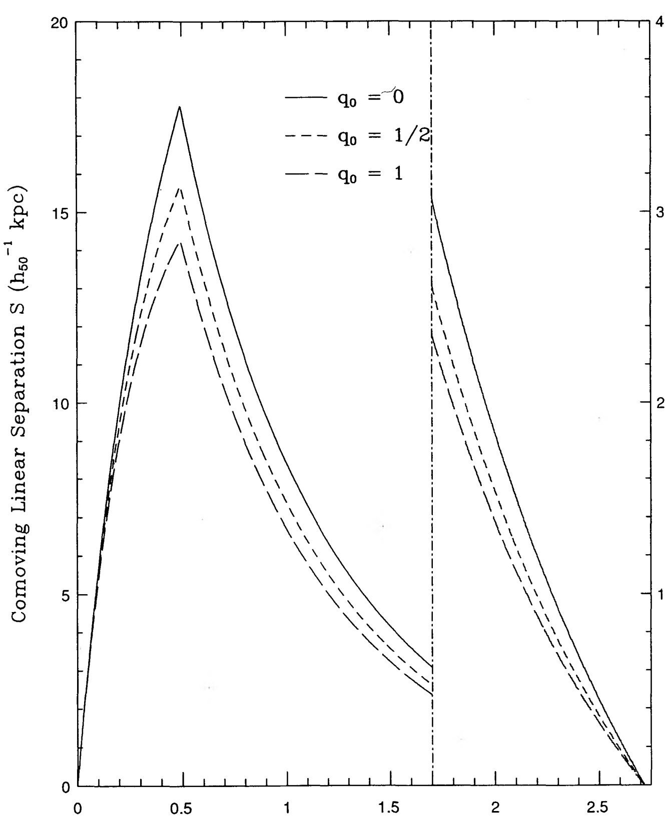

FIG. 4.—Separation between the two beams as a function of redshift for the gravitational lens system UM 673.

example, by the models of Tytler or Pettini et al., the two lines of sight would have crossed *different* clouds at the same redshift, since their size (0.3 or 10^{-5} pc) would be very small compared with the separation between the light beams (typically 1 kpc), and no correlation between the measured equivalent widths would be expected.

Thin sheets are still possible, but they would have to have axial ratios of 10^4–10^8 and be homogeneous on scales of $3h_{50}^{-1}$ pc to $2000h_{50}^{-1}$ pc (the separation between the light beams for the extreme Lyα clouds of our sample).

There is also strong evidence that the equivalent widths of the Lyα lines, as given by Foltz et al. (1984) correlate also in the case of Q2345+007, as shown in Figure 6. In consequence, the scale values given above should be increased up to $22h_{50}^{-1}$ kpc (if the deflector redshift is 1.5), and another order of magnitude should be added to the axial ratios in the case of thin sheets.

4.2.3. *Limits on the Diameter of the Lyman-Alpha Clouds: Monte Carlo Simulations*

In this section we shall compare the number of anticoincidences with the total number of lines in our sample in order to put some constraints on the size of the Lyα clouds. We shall then try to use the information given by the equivalent widths of the lines to set constraints on the possible structure of Lyα clouds.

In the following we shall use a simple model: we assume that the clouds are all identical (no evolution) and spherical.

First, we define the ratio f between the number of anticoincidences and the sum N of the number of anticoincidences and the number of coincidences, for different values of the diameter, D. We can then compare the observational results with those from Monte Carlo simulations, whose description follows:

a) We use the observed distribution of Lyα clouds along the line of sight, in the sense that we put spherical clouds at each of the redshifts derived for the (single) lines in the observed spectra.

b) Working in the plane perpendicular to the line of sight, we compute f for each assumed value of $R_c = D/2$ in the following way (see also Fig. 7): (i) the projection of a spherical cloud on a plane perpendicular to the line of sight is a disk: we consider the center of this disk to be the origin of the coordinates; (ii) for each Lyα line, the separation $S(z_i)$ between the light beams is computed using equation (1); (iii) two points, $\boldsymbol{r}_{A,i}$ and $\boldsymbol{r}_{B,i}$, separated by $S(z_i)$ are randomly chosen on a region covering a disk of radius at least equal to $R_c + S(z_i)$, such that their distributions are uniform on this disk, and the corresponding impact parameters $r_{A,i}$ an $r_{B,i}$ are computed; (iv) $r_{A,i}$ and $r_{B,i}$ are then compared with R_c: (1) if only one of $r_{A,i}$ or $r_{B,i}$ is greater than R_c, the number of anticoincidences is increased by one; (2) if $r_{A,i}$ and $r_{B,i}$ are smaller than R_c, the number of coincidences is increased by one; (3) if both $r_{A,i}$ and $r_{B,i}$ are greater than R_c, the trial is not counted at all.

We also made similar simulations for an oblate spheroid, given by the equation

$$\frac{x^2 + y^2}{a^2} + \frac{z^2}{b^2} = 1 , \qquad (5)$$

without any preferential direction for any axes. In particular, if b/a is very small, we have a simple model for a circular sheet.

For N lines, this process is repeated a sufficient number of times in order to get accurate results for f and the associated

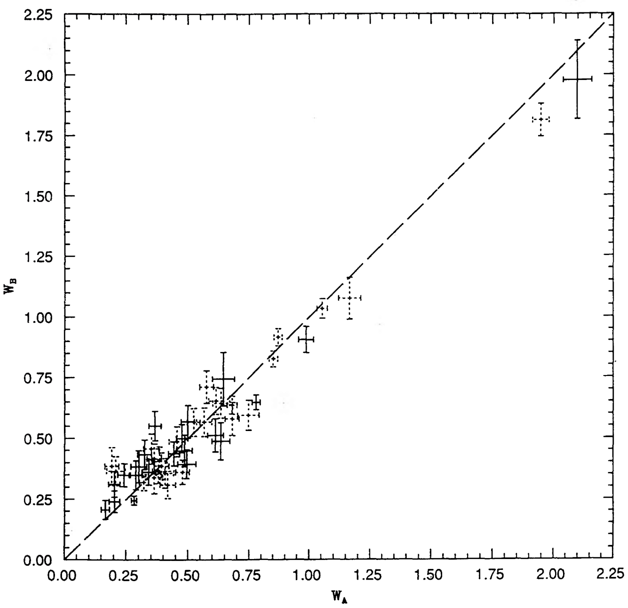

FIG. 5a

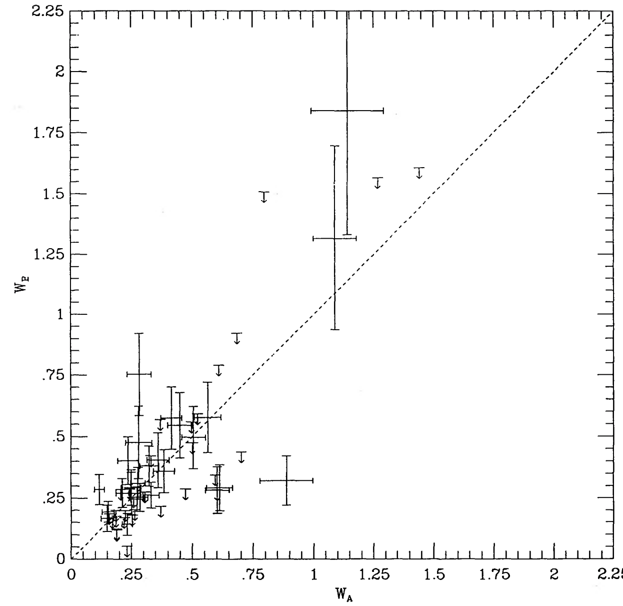

FIG. 5b

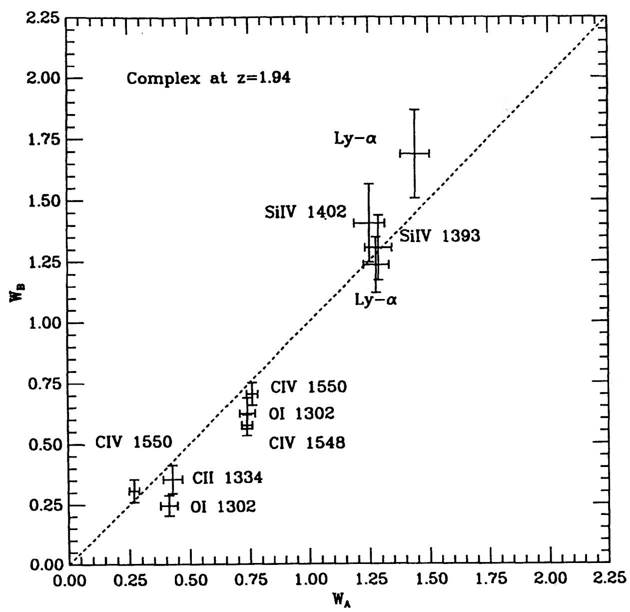

FIG. 5c

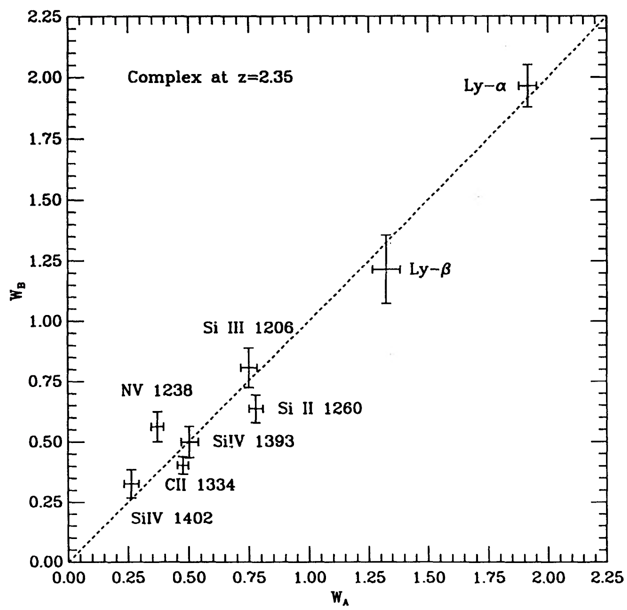

FIG. 5d

FIG. 5.—Correlation between rest equivalent widths of coincidence lines in the 2 Å spectra, (*a*) for the 21 single (*solid-line symbols*) and the 26 blended Lyα lines (*dashed-line symbols*); (*b*) for the 3 σ level detected lines in spectrum B and the 5 σ level detected lines in spectrum A, and the 3 σ upper limit on W_B for the "missing" lines; (*c*) the $z_{\rm abs} = 1.94$ heavy-element complex, including the upper limit on W_B for the missing line in spectrum B; (*d*) the $z_{\rm abs} = 2.35$ heavy-element complex, including the upper limit on W_B for the "missing" lines in spectrum B. All equivalent widths are in angstroms.

errors. The choice of the line sets has two effects: first, generally, if N increases, the errors get smaller; second, since we use the observed lines to obtain the distribution of the clouds in our simulations, a different set of lines (but with the same value for N) will usually produce different results. However, adding more clouds close to the quasar does not affect the results significantly if the separation between the light beams is much smaller than the size of the clouds.

Some results from these simulations are presented in Figure 8 as plots of $f + 2\sigma$ and $f - 2\sigma$ versus D. In turn, for a given observed value $f_{\rm obs}$, we obtain 2 σ *lower* and *upper* limits for D. The whole set of results is discussed below and summarized in Table 3, for different samples and for the two cases.

For case 1, i.e., that the two anticoincidences are Lyα lines, we have the following:

a) Sample 1 is constituted from the isolated lines alone. It forms the most secure sample: its 21 coincidence lines and one anticoincidence line are not affected by blending, and therefore there is a one-to-one correspondence between the lines and

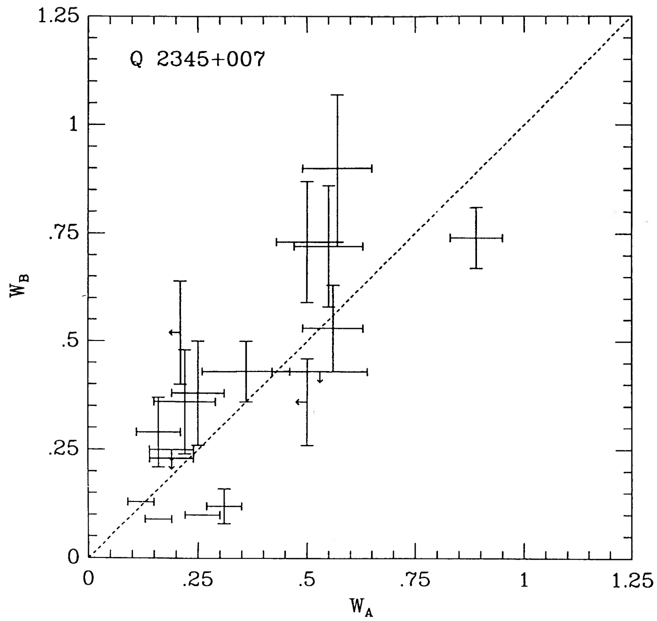

FIG. 6.—W_B vs. W_A for Q2345+007 images A and B. Rest equivalent widths in angstroms.

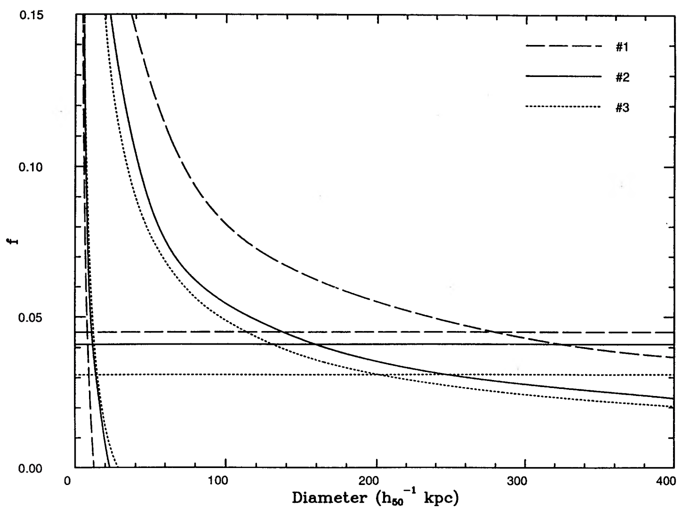

FIG. 8.—Plot of $f - 2\sigma$ and $f + 2\sigma$ vs. D for samples 1, 2, and 3. The horizontal lines mark the observed values of f for the three samples; their intersections with the curves give the 2 σ limits on the cloud sizes.

their equivalent widths in the high-resolution spectra and the 2 Å spectrum of A. We obtain a 2 σ lower limit of $8h_{50}^{-1}$ kpc and a 2 σ upper limit of $280h_{50}^{-1}$ kpc.

b) Sample 2 contains the 21 isolated and 26 blended coincidence lines, and the one isolated and one blended anticoincidence line. We consider the results ($12h_{50}^{-1}$ kpc for the 2 σ lower limit and $160h_{50}^{-1}$ kpc for the 2 σ upper limit) as the best (the most convincing) values we can obtain with our data: we use the blended lines in the same way as for the single ones. This is equivalent to saying that (i) one subcomponent of a blended line is surely present in the A and in the B spectra, and (ii) nothing is known about the detection of the other ones, for the B spectrum signal-to-noise ratio is not as good as that for the A spectrum.

c) Sample 3 is an attempt to use all the information of the high-resolution spectra. To the 21 single lines, we have added all the subcomponents of the blended lines whose equivalent widths (as measured in the high-resolution spectra) are bigger than twice the formal errors on the equivalent widths of the corresponding B lines. With such a criterion, we use as many lines as possible, while we do not take into account the very low equivalent width lines whose absence is unnoticed because of the noise of the 2 Å spectra. We obtain 62 coincidence lines, and we assume that there are two anticoincidences. The 2 σ lower and upper limits are therefore $21h_{50}^{-1}$ kpc and $200h_{50}^{-1}$ kpc.

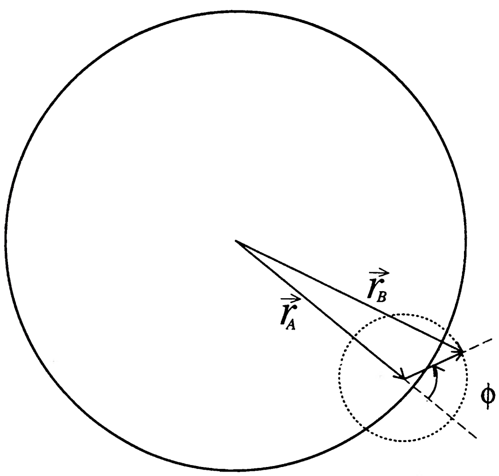

FIG. 7.—Schematic diagram related to the Monte Carlo simulations; the symbols are described in the text.

d) Sample 4 is the same as sample 2, but for oblate spheroidal clouds. We find that the results—a 2 σ lower and upper limit for $2a$ of $20h_{50}^{-1}$ kpc and $300h_{50}^{-1}$ kpc, respectively—are independent of b/a if this ratio is less than 0.1, owing to the relatively small number of lines. These values are about twice those obtained for a spherical Lyα cloud.

e) Sample 5 comes from the results of Foltz et al. (1984). From the 19 lines published, we removed lines 8, 11, and 12 because of Note 5 of their table, while line 19 has a larger redshift than that assumed for the quasar and, therefore, cannot be used in our model. We are left with 13 coincidence and two anticoincidence lines. We assume a redshift of 0.5 for the lens. Although we make a better use of the sample, we obtain only a slightly larger value for the 2 σ lower limit ($8h_{50}^{-1}$ kpc instead of $5h_{50}^{-1}$ kpc) because of their error on the formula giving the separation between the two lines of sight, mentioned in § 4.2.1. However, we can also set a 2 σ upper limit of $104h_{50}^{-1}$ kpc.

f) Sample 6 is the combination of samples 2 and 5. Compared with sample 5, this increases significantly the 2 σ lower limit to $13h_{50}^{-1}$ kpc, while the 2 σ upper limit decreases to $92h_{50}^{-1}$ kpc.

g) Samples 7 and 8 (and samples 9 and 10) are obtained with the same data set as for samples 5 and 6, except that the redshift for the lens in the Q2345+007 system is assumed to be $z = 1$ ($z = 1.5$). Comparing samples 2 and 8, we see that the Q2345+007 data help to improve the 2 σ lower limit to $24h_{50}^{-1}$ kpc, but not the upper limit (which stays at about $160h_{50}^{-1}$ kpc). When samples 2 and 10 are compared, we find that the 2 σ lower limit is increased to $54h_{50}^{-1}$ kpc. However, the 2 σ upper limit is significantly less restrictive in sample 10 ($360h_{50}^{-1}$ kpc) than in sample 2 ($160h_{50}^{-1}$ kpc).

TABLE 3

2 σ LIMITS ON THE SIZE OF LYMAN-ALPHA CLOUDS

CASE 1: ANTICOINCIDENCES ARE Lyα LINES				CASE 2: ANTICOINCIDENCES ARE A Mg II DOUBLET			
Sample Number	Description	f	Diameter (h_{50}^{-1} kpc)	Sample Number	Description	f	Diameter (h_{50}^{-1} kpc)
			A. Samples from UM 673 Only				
1	21 single lines; 1 anticoincidence	0.045	$8 < D < 280$	13	20 single lines; no anticoincidences	0	...
2	26 blended lines; 21 single lines; 2 anticoincidences	0.041	$12 < D < 160$	14	24 blended lines; 20 single lines; no anticoincidences	0	$23 < D$
3	62 subcomponents; 2 anticoincidences	0.031	$21 < D < 200$	15	61 subcomponents; no anticoincidence	0	$28 < D$
4	As sample 2; spheroidal clouds	0.041	$20 < 2a < 300$	16	As sample 14; spheroidal clouds	0	$40 < 2a$
			B. Samples from Q2345+007 Only or with UM 673				
5	13 lines; 2 anticoincidences; z_D(Q2345+007) = 0.5	0.133	$8 < D < 104$	...	...	...	...
6	Sample 2 + sample 5	0.062	$13 < D < 92$	17	Sample 14 + sample 5	0.034	$20 < D < 260$
7	13 lines; 2 anticoincidences; z_D(Q2345+007) = 1.0	0.133	$26 < D < 330$	...	...	...	...
8	Sample 2 + sample 7	0.062	$24 < D < 162$	18	Sample 14 + sample 7	0.034	$35 < D < 480$
9	13 lines; 2 anticoincidences; z_D(Q2345+007) = 1.5	0.133	$62 < D < 770$	...	...	...	...
10	Sample 2 + sample 9	0.062	$54 < D < 360$	19	Sample 14 + sample 9	0.034	$80 < D < 1000$
11	13 lines; 2 anticoincidences; Q2345+007 is not a GL	0.133	$500 < D < 6500$	...	...	...	...
12	Sample 2 + sample 11	0.062	$410 < D < 3400$	20	Sample 14 + sample 11	0.034	$380 < D$

h) Samples 11 and 12 are the same as sample 5 and 6, except that we suppose that Q2345+007 is not a gravitational lens system, but a real quasar pair as proposed by Steidel & Sargent (1990). With the same data, we obtain a 2 σ lower limit of $500h_{50}^{-1}$ kpc, instead of $100h_{50}^{-1}$ kpc as they obtained in their paper, for the reason explained in paragraph *e* above. However, the comparison between samples 2 and 12 shows that the results are incompatible: the 2 σ upper limit obtained with sample 2 is much smaller ($160h_{50}^{-1}$ kpc) than the 2 σ lower limit given in sample 12 ($410h_{50}^{-1}$ kpc).

We conclude that if the two anticoincidences are indeed Lyα lines, the results from UM 673 alone are not compatible with the results obtained under the hypothesis that Q2345+007 is a binary quasar. In this case, the size of Lyα clouds is small enough so that two relatively close, nearly parallel light paths, as in the case of a binary quasar, would cross different Lyα clouds. Therefore, study of the Lyα forest can help to discriminate between the binary quasar and the gravitational lens explanations for close images of high-redshift quasars.

We present also the results for case 2, in which the anticoincidences are in fact due to a Mg II doublet, with a Mg I line detected at the same z. The major differences are that the 2 σ lower limits are larger and that no upper limits can be set. In conclusion, if the two anticoincidences are caused by a Mg II doublet—in fact, even if one of the anticoincidences is not a Lyα line but a metallic line in a not-yet-identified system—we are unable to give any meaningful 2 σ upper limit for the diameter of the Lyα clouds, using the results from UM 673 alone. As a consequence, they are compatible with any of the possible hypotheses as to the origin of Q2345+007. In particular, in the case of the binary quasar explanation, we are led to a 2 σ lower limit for the Lyα cloud diameter of the order of $400h_{50}^{-1}$ kpc.

4.2.4. *Structure of the Lyman-Alpha Clouds*

The fact that the equivalent widths of absorption lines detected in the two spectra correlate proves that Lyα clouds are structured, in the sense that the column density and the velocity dispersion at a given impact parameter set important constraints on these quantities at another one. In the case of UM 673, the column densities and the velocity dispersion must have very similar values for impact parameter differences between $0h_{50}^{-1}$ and $2h_{50}^{-1}$ kpc, except if in each case—corresponding to rest equivalent widths ranging from 0.2 to 2 Å—the variation of one of the parameters is well counterbalanced by the appropriate change of the other parameter (that is very unlikely).

On the other hand, nearly any density profile in a cloud produces a variation of the column density with the impact parameter, as recalled by Milgrom (1988). The fact that the equivalent widths of the two anticoincidences are among the lowest in our sample (assuming they are Lyα lines) suggests actually that Lyα clouds are not of uniform density.

The way the equivalent widths of absorption lines detected in the two spectra correlate gives us a tool to study the structure of the Lyα clouds, as we shall demonstrate in this section by using a simple model: we assume that the Lyα clouds are described by a singular isothermal sphere, whose projected surface density at an impact parameter r is given by

$$\Sigma(r) = k \frac{R_c}{r} ; \quad (6)$$

where k can be written as $k = \sigma_{\parallel}^2/2G$ kpc; $\sigma_{\parallel}$ is the one-component central velocity dispersion; and G is the gravitational constant.

We then compute the equivalent width of a line using the (simplified) relation

$$W(r) = W_0(1 - e^{-\tau\Sigma(r)}) , \quad (7)$$

where W_0 is the equivalent width of a line for which r is 0 (i.e., the light crosses the center of the cloud); τ is a parameter which takes into account the opacity of the cloud. In our simple model, W_0 and the product τk are adjusted in order to match the observed distribution of equivalent widths. With the restriction that it must be larger than the maximum value of W in the sample, the precise value of W_0 does not much change the following results, since the range of r-values for which large equivalent widths (between W_0 and the largest value of W) are produced is very small compared with R_c, which is now the value of the impact parameter giving rise to a line whose equivalent width has the lowest value in our sample. This relation is a reasonable approximation for clouds with opacity up to ~ 1.

Using the distribution in redshifts of the single lines, we can compute the probability density $P(W_A, W_B)$ of having a line whose equivalent width in spectrum A is W_A, while the one for its corresponding line in spectrum B is W_B. The logarithm of $P(W_A, W_B)$ is presented in Figure 9*a* for $R_c = 5h_{50}^{-1}$ kpc and in Figure 9*b* for $R_c = 20h_{50}^{-1}$ kpc. The discrete structure of the probability density is caused by the discrete distribution of the separation between the light beams at the redshift of the Lyα clouds. The inner pattern is produced by the clouds closest to the quasar, while the widest pattern is due to the most remote ones. The probability is very high for the low values of equivalent widths, but with a very small dispersion along the line $W_A = W_B$; the dispersion increases more and more along the line of equal equivalent widths, limited by two asymptotic branches. On the other hand, the dispersion is much larger for $R_c = 5h_{50}^{-1}$ kpc than for $R_c = 20h_{50}^{-1}$ kpc; in other words, the allowed region, i.e., the number of possible combinations of (W_A, W_B), is much larger for smaller values of R_c.

Such behavior can easily be explained: the ratio of equivalent widths between a line in spectrum A and the corresponding line in spectrum B is sensitive to the density gradient of the cloud. If a line is produced near the center of a cloud, it is very unlikely that its equivalent width will be very similar to that of the corresponding line in the other spectrum, if the typical separation between the light beams is greater than about $0.05R_c$ to $0.1R_c$ (as one can see in comparing Figs. 9*a* and 9*b*), since the probability that impact parameters are equal (or have similar values) is much smaller than the probability that they are very different (relative to the cloud size). This produces a dispersion of the points in a graph of W_B versus W_A, which is very similar to a noncorrelation if the number of points is small. A strong correlation between equivalent widths of coincidences is then expected only if the typical radius of a cloud is much larger than the typical separation between the light beams. Note that graphs with similar properties can be produced for spherical clouds whose equivalent width decreases more quickly than linearly with R_c.

The observed correlation between W_A and W_B is then once more remarkable. This means the following:

a) Both light beams actually cross the same clouds.

b) The typical radius of a cloud R_c is much larger than the typical separation ($1h_{50}^{-1}$ kpc) between the light beams, since

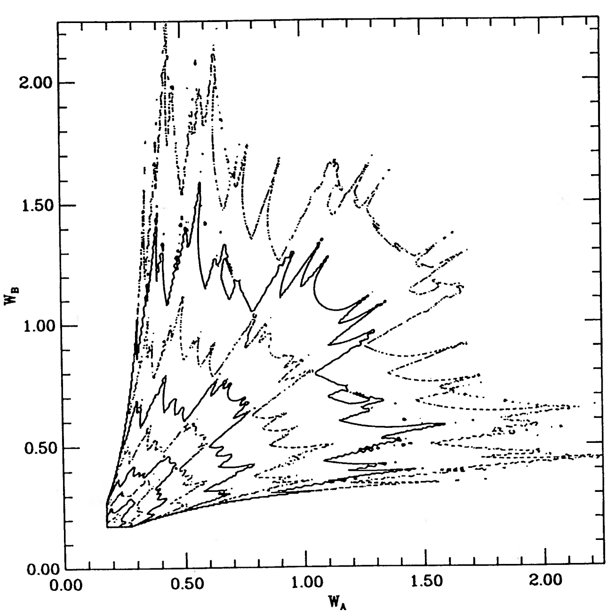

FIG. 9*a*

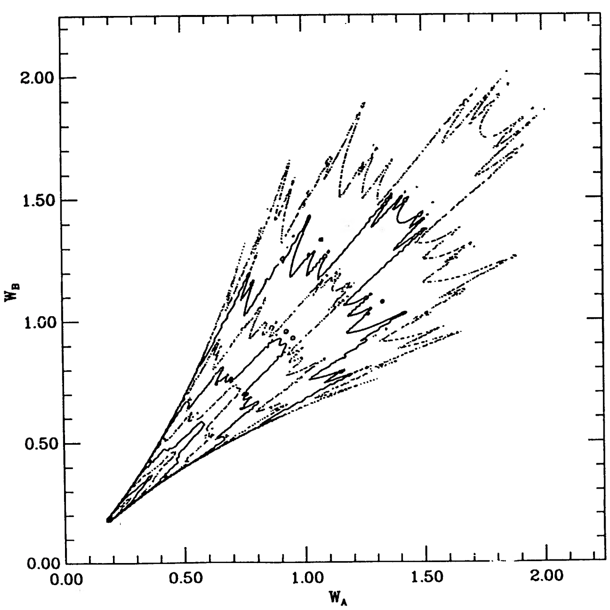

FIG. 9*b*

FIG. 9.—Logarithm of the probability that a line of equivalent width W_A occurs in spectrum A when one of W_B occurs in spectrum B, for an isothermal sphere: (*a*) with $R_c = 5h_{50}^{-1}$ kpc; (*b*) with $R_c = 20h_{50}^{-1}$ kpc. Contour plots are -7.5 to 0, with steps of 0.5. Contours for lower probabilities are not shown.

the dispersion of the points is still compatible with zero; a maximum-likelihood determination gives a lowest value of about $50h_{50}^{-1}$ kpc with the single lines, which should be taken only as indicative, because of the very small dispersion of the observed points.

c) As a consequence of item *b*, the available data are not yet sufficient to determine the value of R_c and the density profile for spherical Lyα clouds.

4.2.5. *Clumpiness of the Lyman-Alpha Clouds*

The very good correlation observed between the equivalent widths of the lines detected in both spectra means that the two light beams actually cross the same clouds, but does not exclude the possibility that they are clumpy. Let us make some simple assumptions. As an extreme case, we use a model where a Lyα cloud is composed of a very large number of small individual cloudlets in an empty "intercloudlet" medium. First we assume that a given cloudlet contributes an amount W_c (in mean) to the (total) equivalent width of a Lyα line, i.e., that the cloudlets and the clouds are optically thin. Hence, we may write $W_A = n_c^A W_c$ and $W_B = n_c^B W_c$, where n_c^A and n_c^B are the numbers of cloudlets in one cloud on the lines of sight to images A and B, respectively. Second, we can say that, within the same *cloud*, the light paths to A and B are comparable, so that n_c^A and n_c^B should both fall in a range $[n_c - \sigma_{n_c}, n_c + \sigma_{n_c}]$, where n_c is the mean number of cloudlets in the region probed by the light beams. (In this case we interpret the observed correlation between the equivalent widths W_A and W_B as due to a very large number of cloudlets.) We can assume that the number of cloudlets encountered along the line of sight to an image follows Poisson statistics, so that $\sigma_{n_c} = (n_c)^{1/2}$. Finally, because of the measurement errors, we have: $\sigma^2_{\log(W_A/W_B)} > \sigma_{\log(n_c{}^A/n_c{}^B)}$, which gives $n_c > 2/\sigma^2_{\log(W_A/W_B)}$. In this way, the dispersion observed in Figure 5 could be interpreted as being due partly to the clumpiness of the cloud. Numerically, $n_c > 550$, so that we obtain a roughness factor $\sigma_{n_c}/n_{n_c} < 0.04$, corresponding to statistical Poissonian fluctuations if the model is taken literally. If Lyα clouds are more similar to a clumpy continuous medium, the number of clumps can be less numerous. In conclusion, the clouds must be very smooth on scale ranges from $3h_{50}^{-1}$ pc to $2000h_{50}^{-1}$ pc, as an extreme case in terms of differences between the number of clumps encountered along the two lines of sight.

4.3. *Velocity Differences*

Measurements of the velocity difference between two corresponding lines in the spectra of images A and B are also of interest. Dependence of this parameter on the equivalent widths of the lines or on the linear separation and/or redshift will be studied in this section.

4.3.1. *Individual Velocity Differences*

In order to obtain the most precise values of the velocity differences $\Delta V = c(\lambda_A - \lambda_B)/\lambda$, we have used the cross-correlation technique developed by Tonry & Davis (1979) on individual single lines. Each line was first extracted from the spectra, to avoid (or to reduce as much as possible) any contamination of the cross-correlation function by its neighbors. The results are presented in Table 2, together with the formal errors $\sigma_{\Delta V}$. The difference in velocities is equal to zero within the error bars, except in very few cases: (*a*) the nonzero value of ΔV for the line at 3726 Å is very probably due to the line shape at zero intensity; (*b*) nonzero differences are detected at the 2 σ level for the lines at 3792 Å (-9.4 ± 3.5 km s^{-1}), 3991 Å (9.0 ± 3.7 km s^{-1}), and 4372 Å (21 ± 7.8 km s^{-1}). The velocity differences for the blended lines are also essentially compatible with 0 km s^{-1} within the error bars, except for the line at 4259 Å (-11.6 ± 3.0 km s^{-1}).

The histogram of the difference of velocities for the single and blended lines is presented in Figure 10. The standard deviation is found to be 17 km s^{-1}.

No evidence of correlation is found between the equivalent widths and the difference in velocities, which argues against the presence of systematic mass motions linked to density gradients.

4.3.2. *Evolution*

There is no indication of any dependence of the dispersion of the ratio W_A/W_B or of the difference in velocities on the combined effect of the redshift and the separation of the light beams.

We present in Figure 11 the graph of W_A/W_B versus z as an example.

5. ANALYSIS OF THE METALLIC ABSORPTION-LINE SYSTEMS

UM 673 gives new information on the spatial distribution, the column density, and the ionization of the metallic systems, since several metallic absorption-line systems are found or could be expected in our spectra. In order of increasing redshift, they are as follows:

a) $z_{\rm abs} = 0.17$ (redshift of the galaxy D south of UM 673).—No convincing identification could be made; several lines in the bluest part of the 1 Å spectrum could be Mg I λ2852.

b) $z_{\rm abs} = 0.4261$.—This possible system is discussed above. Any confirmation of its existence is very important for the study of the Lyα clouds; if it is real, then the distribution of Mg II varies over scales of $16h_{50}^{-1}$ kpc, similar to that for the 1.483 and 1.491 systems of Q2345+007. This is also to be compared with the small but significant differences found for the C IV lines of the $z_a = 1.1249$ system of the gravitational lens

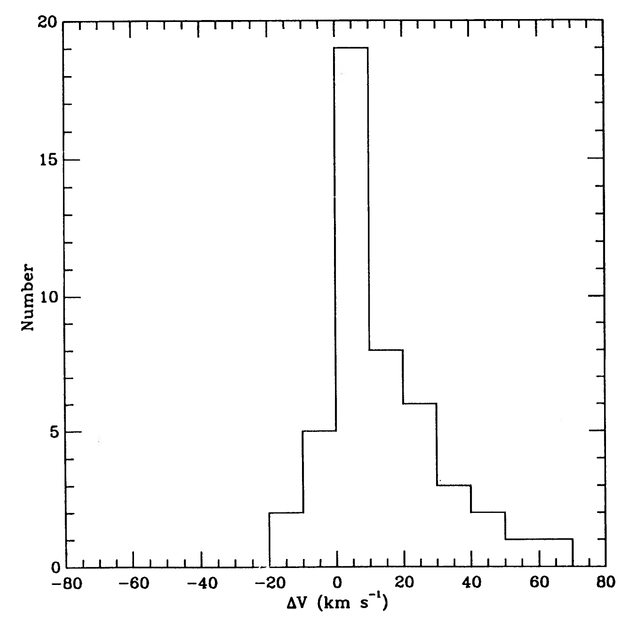

FIG. 10.—Histogram of the difference in velocities for all the Lyα lines

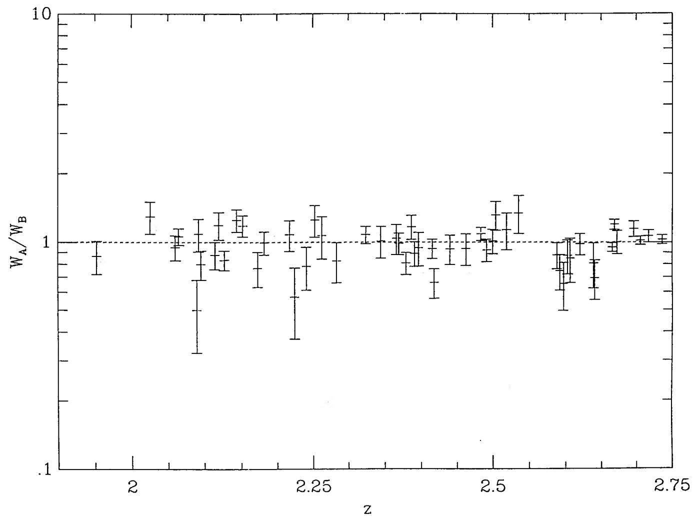

FIG. 11.—$|W_A/W_B|$ vs. z for the single lines

quasar Q0957+561 images A and B (Boksenberg & Sargent 1983), whose line of sight at this redshift are separated by $5.5h_{50}^{-1}$ kpc.

c) $z_{\rm abs} = 0.493$ (redshift of the lensing galaxy).—Ca II H and K lines plus probable Na I D1 and D2, believed to be formed in the lensing galaxy (cf. Paper II). These lines are only detected in component B, closer to the center of the galaxy than A. Our spectra do not detect other associated lines.

d) $z_{\rm abs} = 1.9406, 1.9417, 1.9436, 1.9441$.—Values first reported from SBS. The first two redshift systems, revealed only by C IV lines in SBS are detected in the higher resolution spectra but are blended in the 2 Å spectra. Refer to § 5.1 for more details. Figure 5*c* presents W_B versus W_A for all the 2 Å coincidence lines of this complex.

e) The C IV system at $z_{\rm abs} = 2.3245$ (SBS).—This system does not show any line in the spectral range covered by our data, not even Lyα; in fact the signal-to-noise ratio of our 5000–6000 Å spectrum is not sufficient to detect this doublet either.

f) $z_{\rm abs} = 2.3556, 2.3566$.—First reported in Paper II, then in SBS. This complex system is detected in both 2 Å spectra (see § 5.2). Figure 5*d* presents W_B versus W_A for all the 2 Å coincidence lines of this complex.

The possible $z_{\rm abss} = 1.8987$ system (Paper II) is not confirmed by our new data.

Tables 4A–4G give a summary of the properties of the $z = 1.94$ and $z = 2.35$ complexes, described also below. The best values for the study of the heavy-element systems are of course found in the higher resolution spectra, while an attempt at comparison of the two lines of sight can be made with the 2 Å spectra. In general this is difficult since most of the lines are blended with Lyα or metal lines. Hopefully, we know already that the equivalent widths of the Lyα lines are nearly equal in the A and B spectra.

5.1. *The Complex System at* $z_{\rm abs} = 1.94$

Nine lines are detected at the 5 σ level in the 2 Å spectra of both components A and B. The four subcomponents are revealed mainly by their C IV doublets, which are responsible for the complicated structure of the involved lines. For example, C IV λ1548 of the $z = 1.9441$ system falls on the wing of C IV λ1550 of the $z = 1.9406$ system. The O I λ1302 line is probably detected for all the subcomponents. The C II λ1334 line is found only in the 1.9406 and 1.9417 systems. The Si IV doublet is only possibly detected in the 1.9417 system, but is unambiguous in the 1.9406 one. Other metallic lines (Al II λ1670, Si II λ1260, and possibly Si II λ1193, Si III λ1206) are found only in the latter system. Except perhaps for the Si II lines, there is no significant difference between the equivalent widths in the A and B 2 Å spectra. Velocity differences are also equal to zero within the error bars.

We may conclude that there is no dramatic change in the column density of the region which gives rise to this system on scales of $2.1h_{50}^{-1}$ kpc. It is worthwhile to remember that there are differences on larger scales ($10h_{50}^{-1}$ kpc to $91h_{50}^{-1}$ kpc, depending on the redshift of the lensing galaxy) for the 1.483 and 1.491 systems of Q2345+007 (Tyson et al. 1986).

5.2. *The Saturated Lyman-Alpha System at* $z_{\rm abs} = 2.3556, 2.3566$

Seven lines are detected in both spectra, and six lines are detected only in the spectrum of image A for this complex. The identification of the O VI lines is far from certain; we mention it because of the expected equivalent width ratio and of the poorer wavelength calibration in the bluest part of the 1 Å spectrum. If they are confirmed, then the two light beams probe regions with different ionization states. We note that Lyγ is detected in the 2 Å spectrum of A and is also present at the 3 σ level in the spectrum of B. The existence of two components separated by 300 km s^{-1} is ascertained by the double structure of the Si II λ1260, Si III λ1206, Si IV, and C IV lines. The N I $\lambda\lambda$1134 and 1200 and the N II λ1083 lines are detected only in the $z = 2.3566$ system. There is no significant difference between the equivalent widths of the lines of this complex between the 2 Å spectrum of images A and B. We attribute the significant difference of velocities between the Lyα lines in both 2 Å spectra as due to the shape of the line at zero intensity: if it were real, such a difference would have been expected also for the Lyβ lines. Otherwise, the difference in velocities between corresponding lines in the two spectra is comparable with zero within the error bars.

6. CONCLUSIONS

The size of Lyα clouds is a basic parameter required to understand their nature and eventually their origin. An upper limit of $800h_{50}^{-1}$ kpc has been fixed by the observations of relatively close pairs of quasars (Shaver & Robertson 1983). However, gravitational lenses offer to probe the Lyα clouds on much smaller scales. A first lower limit was obtained with PG 1115+080 (Weymann & Foltz 1983), then improved with the lens system Q2345+007 (Foltz et al. 1984). Unfortunately, because of the faintness of the images and because the deflector has not yet been identified, it is not possible to exploit the latter case fully. However, it is interesting to note that a correlation between the rest equivalent widths of the coincidences does exist in this case too. UM 673 is more useful, in spite of a smaller separation between the light beams.

The results of our analysis of the spectra of the gravitational lens system UM 673 images A and B are given below.

6.1. *For the Lyman-Alpha Cloud Lines and the Metallic System Lines*

a) All the 68 lines detected at 5 σ in the spectrum of the fainter component appear also in the spectrum of the brighter one. Because of the difference in the signal-to-noise ratio, the opposite is not true; however, a number of "missing" lines at

1992ApJ...389...39S

TABLE 4A

HEAVY-ELEMENT SYSTEM AT z_{abs} = 1.9406

	B (2 Å)				A (2 Å)			A (1 Å)			A (0.6 Å)			A (0.33 Å)			
	λ	W_{res}	z	ΔV	λ	W_{res}	z	λ	W_{res}	z	λ	W_{res}	z	λ	W_{res}	z	ION
B[a]	(3506.85	0.32±0.10	1.9388)		3506.70	0.87±0.11	1.9387	3508.57	0.095±0.003	1.9402							?Si II λ1193
S	(3547.84	0.57±0.14	1.9406)		3548.10	0.56±0.05	1.9408	3548.17	0.65±0.01	1.9409							Si III λ1206
B	3574.06	1.23±0.12	1.9400	+8.80±15.9	3574.24	1.28±0.05	1.9401	3574.05	1.33±0.01	1.9400							Lyα
B		0.29			3706.87	0.49±0.04	1.9410	3706.47	0.27±0.01	1.9406							Si II λ1260
														3828.85	0.24±0.03	1.9404	O I λ1302
B	3924.61	0.36±0.06	1.9408	−5.80±24.2	3924.29	0.43±0.04	1.9406	3924.55	0.55±0.01	1.9408				3924.34	0.39±0.02	1.9406	C II λ1334
B	4096.78	1.31±0.13	1.9394	[b]	4096.69	1.29±0.05	1.9393	4098.30	0.72±0.01	1.9405	4098.05	0.37±0.03	1.9403	4098.21	0.59±0.02	1.9404	Si IV λ1393
B	4122.59	1.40±0.16	1.9389	+44.8±54.9	4123.17	1.25±0.06	1.9393	4124.10	0.28±0.01	1.9400	4124.91	0.41±0.03	1.9405	4125.10	0.31±0.01	1.9407	Si IV λ1402
B	4552.97	0.57±0.04	1.9408	−12.4±7.70	4552.52	0.74±0.02	1.9405				4552.38	0.53±0.02	1.9404	4552.79	0.510±0.007	1.9407	C IV λ1548
B	4559.71	0.70±0.05	1.9403	−6.50±29.2	4559.33	0.76±0.02	1.9400				4559.91	0.38±0.02	1.9404	4560.29	0.435±0.007	1.9406	C IV λ1550
											4913.06	0.34±0.05	1.9406				Al II λ1670
			1.9400				1.9400			1.9404			1.9404			1.9406	

[a] See explanation of first column of Table 2, given in the Note to Table 2.
[b] The cross-correlation function presents two peaks of nearly equal intensity corresponding to $\Delta V = -70.5 \pm 15.8$ km s^{-1} and 40.3 ± 23.4 km s^{-1}.

TABLE 4B

HEAVY-ELEMENT SYSTEM AT z_{abs} = 1.9417

	B (2 Å)				A (2 Å)			A (1 Å)			A (0.6 Å)			A (0.33 Å)			
	λ	W_{res}	z	ΔV	λ	W_{res}	z	λ	W_{res}	z	λ	W_{res}	z	λ	W_{res}	z	ION
B	3578.79	1.67±0.18	1.9439	−3.1±17.1	3578.89	1.44±0.06	1.9440	3578.55	1.49±0.02	1.9437							Lyα
B	3832.39	0.62±0.06	1.9431	+4.70±9.00	3832.17	0.74±0.03	1.9429	3831.51	0.445±0.007	1.9424				3830.96	0.70±0.03	1.9420	? O I λ1302
B	3924.61	0.36±0.06	1.9408	−5.80±24.2	3924.29	0.43±0.04	1.9406	3924.55	0.55±0.01	1.9408				3925.76	0.07±0.01	1.9418	C II λ1334
B	4096.78	1.31±0.13	1.9394	[a]	4096.69	1.29±0.05	1.9393				4100.27	0.22±0.02	1.9419	4099.67	0.14±0.01	1.9415	? Si IV λ1393
B	4122.59	1.40±0.16	1.9389	+44.8±54.9	4123.17	1.25±0.06	1.9393	4126.03	0.43±0.01	1.9413	4126.54	0.09±0.02	1.9417	4126.53	0.18±0.01	1.9417	? Si IV λ1402
B	4552.97	0.57±0.04	1.9408	−12.4±7.7	4552.52	0.74±0.02	1.9405				4554.00	0.129±0.007	1.9415	4554.32	0.184±0.003	1.9417	C IV λ1548
B	4559.71	0.70±0.05	1.9403	−6.50±29.2	4559.33	0.76±0.02	1.9400				4561.58	0.08±0.01	1.9415	4561.99	0.119±0.003	1.9417	C IV λ1550
$\bar{z}$			1.9410				1.9409			1.9415[b]			1.9416			1.9417	

[a] The cross-correlation function presents two peaks of nearly equal intensity corresponding to $\Delta V = -70.5 \pm 15.8$ km s^{-1} and 40.3 ± 23.4 km s^{-1}.
[b] The Lyα line was not used to compute the mean redshift.

TABLE 4C

HEAVY-ELEMENT SYSTEM AT z_{abs} = 1.9436

	B (2 Å)				A (2 Å)			A (1 Å)			A (0.6 Å)			A (0.33 Å)			
	λ	W_{res}	z	ΔV	λ	W_{res}	z	λ	W_{res}	z	λ	W_{res}	z	λ	W_{res}	z	ION
B	3578.79	1.67±0.18	1.9439	−3.1±17.1	3578.89	1.44±0.06	1.9440	3578.55	1.49±0.02	1.9437							Lyα
B	3837.50	0.24±0.04	1.9470	+13.00±23.70	3836.75	0.41±0.03	1.9464	3834.13	0.48±0.02	1.9444				3833.01	0.53±0.05	1.9436	? O I λ1302
B	4559.71	0.70±0.05	1.9451	−6.50±29.2	4559.33	0.76±0.02	1.9449				4556.95	0.15±0.01	1.9434	4557.30	0.061±0.003	1.9436	C IV λ1548
B	4565.23	0.31±0.05	1.9438	+13.90±16.40	4565.48	0.27±0.02	1.9440							4564.89	0.024±0.003	1.9436	C IV λ1550
$\bar{z}$			1.9449				1.9448			1.9440			1.9434			1.9436	

TABLE 4D

Heavy-Element System at $z_{abs} = 1.9441$

	B (2 Å)				A (2 Å)			A (1 Å)			A (0.6 Å)			A (0.33 Å)			
	λ	W_{res}	z	ΔV	λ	W_{res}	z	λ	W_{res}	z	λ	W_{res}	z	λ	W_{res}	z	Ion
S		0.83			3551.73	0.60±0.06	1.9438	3551.79	0.57±0.01	1.9439							Si III λ1206
B	3578.79	1.67±0.18	1.9439	−3.1±17.1	3578.89	1.44±0.06	1.9440	3578.55	1.49±0.02	1.9437							Lyα
S	3837.50	0.24±0.04	1.9470	+13.0±23.70	3836.75	0.41±0.03	1.9464	3834.13	0.48±0.02	1.9444				3830.96	0.70±0.03	1.9436	? O I λ1302
B	4559.71	0.70±0.05	1.9451	−6.50±29.2	4559.33	0.76±0.02	1.9449				4558.23	0.15±0.01	1.9442	4558.55	0.180±0.003	1.9444	C IV λ1548
B	4565.23	0.31±0.05	1.9438	+13.90±16.40	4565.48	0.27±0.02	1.9440				4565.61	0.19±0.02	1.9441	4565.96	0.051±0.003	1.9443	C IV λ1550
$\bar{z}$			1.9449				1.9446			1.9440			1.9441			1.9441	

TABLE 4E

Heavy-Element System at $z_{abs} = 2.3556$

	B (2 Å)				A (2 Å)			A (1 Å)			A (0.6 Å)			A (0.33 Å)			
	λ	W_{res}	z	ΔV	λ	W_{res}	z	λ	W_{res}	z	λ	W_{res}	z	λ	W_{res}	z	Ion
	(3264.02	1.84±0.51	2.3562)		3264.66	1.14±0.15	2.3568										Lyγ
		1.26			3279.00	1.02±0.14	2.3561										C III λ977
S	3442.79	1.21±0.14	2.3565	+2.70±12.9	3443.11	1.33±0.06	2.3568	3442.32	1.47±0.02	2.3560							Lyβ
B		0.37			3463.78	0.60±0.08	2.3566	3462.65	0.76±0.02	2.3555							? O VI λ1031
B	(3481.49	0.46±0.11	2.3553)		3481.45	0.38±0.06	2.3552	3482.85	0.35±0.04	2.3566							? O VI λ1037
B		0.19			4005.40	0.22±0.03	2.3566							4004.32	0.071±0.006	2.3557	? Si II λ1193
B+	4049.27	0.80±0.08	2.3562	+2.10±27.20	4049.65	0.75±0.03	2.3565				4048.05	0.25±0.01	2.3552				Si III λ1206
B+	4080.62	1.97±0.09	2.3567	+21.0±4.4	4080.46	1.92±0.04	2.3565	4081.14	1.88±0.01	2.3571	4079.22	0.71±0.04	2.3555				Lyα
B	4229.34	0.63±0.06	2.3555	−9.00±16.80	4229.10	0.78±0.03	2.3553				4229.70	0.31±0.04	2.3556	4229.76	0.188±0.006	2.3558	Si II λ1260
B	4478.70	0.40±0.04	2.3560	−5.00±7.30	4478.97	0.48±0.02	2.3562				4477.94	0.22±0.01	2.3554	4478.25	0.224±0.006	2.3557	? C II λ1334
B	4677.40	0.50±0.07	2.3560	−6.05±9.75	4677.56	0.50±0.04	2.3561				4676.78	0.28±0.01	2.3555	4676.79	0.22±0.01	2.3555	Si IV λ1393
B	4707.58	0.32±0.06	2.3560	−2.00±12.60	4707.40	0.26±0.03	2.3558				4706.78	0.17±0.01	2.3553				Si IV λ1402
$\bar{z}$			2.3559				2.3560			2.3559[a]			2.3554[a]			2.3556	

[a] The Lyα line was not used to compute the mean redshift.

TABLE 4F

Heavy-Element System at $z_{abs} = 2.3566$

	B (2 Å)				A (2 Å)			A (1 Å)			A (0.6 Å)			A (0.33 Å)			
	λ	W_{res}	z	ΔV	λ	W_{res}	z	λ	W_{res}	z	λ	W_{res}	z	λ	W_{res}	z	Ion
	(3264.02	1.84±0.51	2.3562)		3264.66	1.14±0.15	2.3568										Lyγ
		1.26			3279.00	1.02±0.14	2.3561										C III λ977
S	3442.79	1.21±0.14	2.3565	+2.70±12.9	3443.11	1.33±0.06	2.3568	3442.32	1.47±0.02	2.3560							Lyβ
B		0.37			3463.78	0.60±0.08	2.3566	3462.65	0.76±0.02	2.3555							? O VI λ1031
B	(3481.49	0.46±0.11	2.3553)		3481.45	0.38±0.06	2.3552	3482.85	0.35±0.04	2.3566							? O VI λ1037
								3636.75	0.14±0.01	2.3566							N II λ1083
								3808.88	0.08±0.01	2.3569							N I λ1134
								3995.11	0.18±0.01	2.3561				3995.18	0.15±0.01	2.3561	? Si II λ1190
B		0.19			4005.40	0.22±0.03	2.3566	4005.51	0.25±0.01	2.3567				4005.62	0.22±0.01	2.3568	? Si II λ1193
S	(4028.63	0.27±0.06	2.3572)		4028.70	0.21±0.03	2.3572	4028.09	0.23±0.01	2.3567	4027.89	0.31±0.04	2.3566	4028.09	0.25±0.02	2.3567	N I λ1200
B+	4049.27	0.80±0.08	2.3562	+2.10±27.20	4049.65	0.75±0.03	2.3565	4049.39	0.82±0.01	2.2563	4049.79	0.46±0.02	2.3566	4949.64	0.78±0.02	2.3565	Si III λ1206
B+	4080.62	1.97±0.09	2.3567	+21.0±4.4	4080.46	1.92±0.04	2.3565	4081.14	1.88±0.01	2.3571	4082.55	0.54±0.04	2.3583	4081.16	1.72±0.02	2.3571	Lyα
B	4229.34	0.63±0.06	2.3555	−9.00±16.80	4229.10	0.78±0.03	2.3553							4230.96	0.110±0.06	2.3568	Si II λ1260
B	4478.70	0.40±0.04	2.3560	−5.00±7.30	4478.97	0.48±0.02	2.3562				4479.44	0.15±0.01	2.3566	4479.74	0.125±0.003	2.3568	? C II λ1334
B	4677.40	0.50±0.07	2.3560	−6.05±9.75	4677.56	0.50±0.04	2.3561				4678.38	0.18±0.01	2.3567	4678.37	0.22±0.01	2.3567	Si IV λ1393
B	4707.58	0.32±0.06	2.3560	−2.00±12.60	4707.40	0.26±0.03	2.3558				4708.54	0.14±0.01	2.3566				Si IV λ1402
$\bar{z}$			2.3562				2.3562			2.3564			2.3566[a]			2.3566[a]	

[a] The Lyα line was not used to compute the mean redshift.

TABLE 4G

C IV DOUBLET OF THE $z = 2.35$ COMPLEX

λ	W_{res}	z	Ion
5194.97	0.16 ± 0.01	2.3555	C IV λ1548
5203.60	0.13 ± 0.01	2.2555	C IV λ1550
5196.76	0.35 ± 0.02	2.3566	C IV λ1548
5205.39	0.50 ± 0.02	2.3566	C IV λ1550

the 5 σ level are detected at the 3 σ level. Following our definition (§ 3.1), we present evidence for two anticoincident lines.

b) The rest equivalent widths of the lines in spectrum B show a clear correlation with the corresponding lines in spectrum A.

c) The difference in velocities between the corresponding lines is zero within the measurement errors, except for six line pairs, among which two are probably due to the shape of the lines at zero intensity, three have a significance level of less than 2.7 (with a velocity difference less than 21 ± 7.8 km s^{-1}), and one has a significance level of 3.9 (with a velocity difference of 11.6 ± 3.0 km s^{-1}).

6.2. *For the Lyman-Alpha Cloud Lines*

We have used Monte Carlo simulations to obtain a best value for the lower limit of the diameter of Lyα clouds, assuming that the clouds are either spherical or oblate spheroids. We find that the diameter of spherical Lyα clouds must be larger than $12h_{50}^{-1}$ kpc at a 2 σ confidence level. If the two anticoincidences are Lyα lines, then we obtain a 2 σ upper limit of $160h_{50}^{-1}$ kpc. For oblate spheroids with an axis ratio less than 0.1, these values are doubled.

We have further used the equivalent width information as a tool to explore the structure of the clouds, assuming they are isothermal spheres. The correlation between equivalent widths is so good that we were only able to confirm that in this case the size of the Lyα clouds is at least 10 times the typical separation between the light beams. A maximum-likelihood calculation yields a lower limit of $50h_{50}^{-1}$ kpc.

If the Lyα clouds are clumpy we estimate an upper limit to the roughness factor of 0.04. Hence, they must be homogeneous on scales from $3h_{50}^{-1}$ pc to $2000h_{50}^{-1}$ pc, given by the separation between the light beams for the most remote and the closest Lyα clouds. The velocity gradient across the clouds must be very small, but it is not significantly different from that observed for the heavy-element systems on comparable scales.

6.3. *For the Metallic Line Systems*

The complex metallic line systems do not show any significant variations on scales from $0.7h_{50}^{-1}$ to $2.2h_{50}^{-1}$ kpc, at $z = 2.3566$ and $z = 1.9406$, respectively. In particular, the system at $z = 2.356$ appears to be double at 0.6 Å resolution; and it appears that the subcomponents themselves are quite similar. If the halos of galaxies do produce the metallic line systems, then their density and their ionization do not vary significantly over these scales, except perhaps for the Si II lines in the $z = 1.9406$ system. If the two anticoincidences reported in the Lyα forest are due to a Mg II doublet, then the distribution of Mg II varies over scales of $16h_{50}^{-1}$ kpc, comparable to that for the $z = 1.483$ and 1.491 systems of Q2345+007.

6.4. *For the Study of Gravitational Systems*

If the actual size of the Lyα clouds is within the range given above, comparing the Lyα lines of two close quasar images should discriminate between the quasar pair and the gravitational lens hypothesis. In particular, if the two anticoincidences are actually Lyα lines, our results confirm the gravitational lens hypothesis for Q2345+007.

A. S. thanks B. Carswell and specially E. Gosset for discussion, the Φ.V. for support, and M. Faucherre for his help during the edition of the main tables. This research was supported in part by the National Science Foundation under grants AST 87-00741 and 90-01181 (U.S.A.) and in part by contract ARC 90/94-140, "Action de recherche concertée de la Communauté Française" (Belgium). A. S. is grateful to ESO for the studentship under which this work was carried out.

REFERENCES

Banse, K., Grosbøl, P., Ponz, D., Ounnas, C., & Warmels, R. 1988, in Proc. Ninth Santa Cruz Summer Workshop in Astronomy, ed. L. B. Robinson (New York: Springer-Verlag), 431
Blandford, R. D., & Kochanek, C. D. 1987, in Proc. Fourth Jerusalem Winter School for Theoretical Physics, Dark Matter in the Universe, ed. J. Bahcall, T. Piran, & S. Weinberg (Singapore: World-Scientific), 133
Boksenberg, A., & Sargent, W. L. W. 1983, in Proc. 24th Liège Astrophys. Colloq., Quasars and Gravitational Lenses, ed. J. P. Swings (Liège: Institut d'Astrophysique), 500
Bond, J. R., Szalay, A. S., & Silk, J. 1988, ApJ, 324, 627
Carswell, R. F., Lanzetta, K. M., Parnell, H. C., & Webb, J. K. 1991, ApJ, 371, 36
Foltz, C. B., Weymann, R. J., Röser, H.-J., & Chaffee, F. H., Jr. 1984, ApJ, 281, L1
Hogan, C. B. 1987, ApJ, 316, L59
Ikeuchi, S., & Ostriker, J. P. 1986, ApJ, 301, 522
Lake, G. 1988, ApJ, 327, 99
Magain, P., Remy, M., Surdej, J., Swings, J.-P., & Smette, A. 1990, in Proc. Workshop on Gravitational Lensing (Toulouse), ed. Y. Mellier, B. Fort, & G. Soucail (Berlin: Springer-Verlag), 88
Milgrom, M. 1988, A&A, 202, L9
Morton, D. C., York, D. G., & Jenkins, E. B. 1988, ApJS, 68, 449
Pettini, M., Hunstead, R. W., Smith, L. J., & Mar, D. P. 1990, MNRAS, 246, 545
Rees, M. J. 1970, ApJ, 160, L29
———. 1986, MNRAS, 218, 25
Refsdal, S. 1964, MNRAS, 128, 307
Sargent, W. L. W., Boksenberg, A., & Steidel, C. C. 1988, ApJS, 68, 539 (SBS)
Sargent, W. L. W., Young, P., Boksenberg, M., & Tytler, D. 1980, ApJ, 42, 41 (SYBT)
Shaver, P. A., & Robertson, J. G. 1983, ApJ, 268, L57
Smette, A., Surdej, J., Shaver, P. A., Foltz, C. B., Chaffee, F. H., Jr., & Magain, P. 1990, in Proc. Workshop on Gravitational Lensing (Toulouse), ed. Y. Mellier, B. Fort, & G. Soucail (Berlin: Springer-Verlag), 122
Steidel, C. C., & Sargent, W. L. W. 1990, AJ, 99, 1693
Surdej, J. 1990, in Proc. Workshop on Gravitational Lensing (Toulouse), ed. Y. Mellier, B. Fort, & G. Soucail (Berlin: Springer-Verlag), 57
Surdej, J., et al. 1987, Nature, 329, 695 (Paper I)
———. 1988, A&A, 198, 49 (Paper II)
Tonry, J., & Davis, M. 1979, ApJ, 84, 1511
Tyson, J. A., Seitzer, P., Weymann, R. J., & Foltz, C. 1986, AJ, 91, 1274
Tytler, D. 1987, ApJ, 321, 49
Verschueren, W., & Hensberge, H. 1990, A&A, 240, 216
Weymann, R. J., & Foltz, C. B. 1983, ApJ, 272, L1
Young, P., Gunn, J. E., Kristian, J., Oke, J. B., & Westphal, J. A. 1980, ApJ, 241, 507
Young, P., Sargent, W. L. W., Boksenberg, A., & Oke, J. B. 1981, ApJ, 249, 415